National Library of Canada
Bibliothèque nationale du Canada

Canadian Theses Service
Services des thèses canadiennes

Ottawa, Canada
K1A 0N4

CANADIAN THESES

THÈSES CANADIENNES

NOTICE

The quality of this microfiche is heavily dependent upon the quality of the original thesis submitted for microfilming. Every effort has been made to ensure the highest quality of reproduction possible.

If pages are missing, contact the university which granted the degree.

Some pages may have indistinct print especially if the original pages were typed with a poor typewriter ribbon or if the university sent us an inferior photocopy.

Previously copyrighted materials (journal articles, published tests, etc.) are not filmed.

Reproduction in full or in part of this film is governed by the Canadian Copyright Act, R.S.C. 1970, c. C-30.

AVIS

La qualité de cette microfiche dépend grandement de la qualité de la thèse soumise au microfilmage. Nous avons tout fait pour assurer une qualité supérieure de reproduction.

S'il manque des pages, veuillez communiquer avec l'université qui a conféré le grade.

La qualité d'impression de certaines pages peut laisser à désirer, surtout si les pages originales ont été dactylographiées à l'aide d'un ruban usé ou si l'université nous a fait parvenir une photocopie de qualité inférieure.

Les documents qui font déjà l'objet d'un droit d'auteur (articles de revue, examens publiés, etc.) ne sont pas microfilmés.

La reproduction, même partielle, de ce microfilm est soumise à la Loi canadienne sur le droit d'auteur, SRC 1970, c. C-30.

THIS DISSERTATION HAS BEEN MICROFILMED EXACTLY AS RECEIVED

LA THÈSE A ÉTÉ MICROFILMÉE TELLE QUE NOUS L'AVONS REÇUE

NL-339 (r. 86/06)

Canada

THE UNIVERSITY OF ALBERTA

M1 TRANSITION STRENGTH IN THE ^{48}Ca (p,p')$^{48}Ca^{*}$ REACTION

BY

(C) RONALD WILLIAM ANDREW MITCHELL

A THESIS
SUBMITTED TO THE FACULTY OF GRADUATE STUDIES AND RESEARCH
IN PARTIAL FULFILMENT OF THE REQUIREMENTS FOR THE DEGREE OF
MASTER OF SCIENCE
IN
NUCLEAR PHYSICS

DEPARTMENT OF PHYSICS

EDMONTON, ALBERTA
FALL 1986

Permission has been granted to the National Library of Canada to microfilm this thesis and to lend or sell copies of the film.

The author (copyright owner) has reserved other publication rights, and neither the thesis nor extensive extracts from it may be printed or otherwise reproduced without his/her written permission.

L'autorisation a été accordée à la Bibliothèque nationale du Canada de microfilmer cette thèse et de prêter ou de vendre des exemplaires du film.

L'auteur (titulaire du droit d'auteur) se réserve les autres droits de publication; ni la thèse ni de longs extraits de celle-ci ne doivent être imprimés ou autrement reproduits sans son autorisation écrite.

ISBN 0-315-32381-7

THE UNIVERSITY OF ALBERTA

RELEASE FORM

NAME OF AUTHOR :	RONALD WILLIAM ANDREW MITCHELL
TITLE OF THESIS :	M1 TRANSITION STRENGTH IN THE ^{48}Ca (p,p')$^{48}Ca^*$ REACTION
DEGREE :	MASTER OF SCIENCE
YEAR THIS DEGREE GRANTED :	1986

Permission is hereby granted to the UNIVERSITY OF ALBERTA LIBRARY to reproduce single copies of this thesis and to lend or sell such copies for private, scholarly or scientific research purposes only.

The author reserves other publication rights, and neither the thesis nor extensive extracts from it may be printed or otherwise reproduced without the author's written permission.

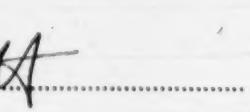

Signature

Permanent Address :
23 Orlon Crescent
Richmond Hill, Ontario
Canada, L4C 6S2

Date : July 15/86

THE UNIVERSITY OF ALBERTA

FACULTY OF GRADUATE STUDIES AND RESEARCH

The undersigned certify that they have read and recommend to the Faculty of Graduate Studies and Research for acceptance a thesis entitled M1 TRANSITION STRENGTH IN THE ^{48}Ca (p,p')$^{48}Ca^*$ REACTION submitted by RONALD WILLIAM ANDREW MITCHELL in partial fulfilment of the requirements for the degree of MASTER OF SCIENCE in NUCLEAR PHYSICS.

Douglas M Sheppard
.....
Supervisor

.....

.....

.....

.....

.....

Date : .....

Abstract

The M1 transition in the ^{48}Ca (p,p')$^{48}Ca^*$ reaction, from the $J^\pi=0^+$ ground state to the $J^\pi=1^+$ excited state at 10.23 MeV, has been studied using the Medium Resolution Spectrometer (MRS) at TRIUMF. Differential cross-sections and analyzing powers were measured at forward angles with incident beam energies of 250, 319, 400 and 500 MeV.

The data are compared with the Independent Particle Model (IPM) calculated microscopically using the density dependent interaction in the Distorted Wave Born Approximation (DWBA). It was found that the IPM correctly describes the angular distribution of the M1 transition differential cross-section, but the IPM strength must be renormalized by a factor of about N=0.3 to agree with experiment, except for the 250 MeV data where a factor of N=0.6 was required.

Two possible models which account for the quenching of the M1 transition strength are presented.

The DWBA calculations do not successfully reproduce the analyzing power measurements.

Acknowledgements

I would like to express my gratitude to both my supervisor Dr. D. Sheppard for his guidance and encouragement during this work and Dr. A. Miller for all of his guidance during the analysis of the experiment.

I would also like to thank Dr. F. Khanna for very useful discussions regarding the theoretical aspects of the experiment, Dr. R. Dymarz for the DWBA calculations and Dr. D. Frekers for all of his help keeping LISA running at the University of Alberta.

Finally, I wish to thank all of the friends I have made in Edmonton for their support and for the pleasure of their company.

Table of Contents

Chapter — Page

1. Introduction 1

2. Theory 5
   2.1 Calculation of Scattering Observables 5
   2.2 Calculation of the Transition Matrix Element (T_{fi}) 5
      2.2a Calculation of T_{fi} using the DWIA 6
      2.2b Calculation of T_{fi} using the Density Dependent Interaction 7
   2.3 Quenching Mechanisms 8
      2.3a The Independent Particle Model (IPM) 8
      2.3b Transitions in a 3-Level System 10
      2.3c Quenching due to Configuration Mixing 12
      2.3d Δ-Nucleon Hole Quenching Mechanism 13

3. Experimental Arrangement 17
   3.1 General Description 17
   3.2 The Medium Resolution Spectrometer (MRS) 17
   3.3 Dispersion Matching 19
   3.4 Beam Line 4B 20
   3.5 On-Line Analysis 20

4. Analysis 30
   4.1 General Description 30
   4.2 The LISA Data Analysis Program 30
   4.3 Replay Analysis 30
      4.3a Coordinate Corrections 30
      4.3b Background Reduction 32
      4.3c Spectra Formation 32
      4.3d Determination of Overall MRS Efficiency 33
   4.4 Calculation of Differential Cross-Section and Analyzing Power 34
   4.5 Statistical Uncertainty in Cross-Section and Analyzing Power 35
   4.6 Normalization 36

4.7 Calibration of Scattering Angle..... 36

5. Results.....43
5.1 ^{48}Ca (p,p')^{48}Ca* at 319 and 400 MeV (January 1985).....43
5.2 ^{48}Ca (p,p')^{48}Ca* at 250 and 500 MeV (October 1985).....45

6. Discussion.....62

References..... 64

Bibliography.....65

Appendix 1. Formal Scattering Theory.....66

Appendix 2. Approximate Methods for Inelastic Scattering.....70

Appendix 3. In-Beam-Polarimeter Properties.....73

Appendix 4. Reaction Kinematics.....75

Appendix 5. Effect of Kinematic Shift on MRS Resolution.....77

Appendix 6. Experimental Data.....78

List of Figures

Figure Page

1.1 Order of nuclear energy levels according to the independent particle model.....4

2.1 Effect of a perturbation V on transitions in a 3-level system.....14
2.2a Excitation energy spectrum of unperturbed 3-level system.....15
2.2b Excitation energy spectrum of 3-level system after perturbation.....15
2.3a M1 strength according to the IPM.....16
2.3b Fragmetation of M1 strength due to configuration mixing.....16
2.3c Transfer of M1 strength between transitions.....16

3.1 General layout of the TRIUMF facility.....22
3.2 The Medium Resolution Spectrometer.....23
3.3 The MRS coordinate system.....24
3.4 Geometry of the MRS focal plane.....25
3.5 Dispersion Matching.....26
3.6 Proton Hall layout showing Beam-Line 4B.....27
3.7 Arrangement of In-Beam-Polarimeter.....28
3.8 Typical on-line focal plane spectrum for the ^{48}Ca (p,p')$^{48}Ca^*$ reaction.....29

4.1 Spectrum showing independence of focal plane position on Y_o.....38
4.2 Spectrum showing independence of focal plane position on θ_{PC}.....39
4.3 Spectrum of Y_I vs. X_I.....40
4.4 Typical focal plane spectrum X_{FPC}.....41
4.5 Energy of outgoing proton after scattering from CH_2 target at 250 MeV.....42

5.1 Differential cross-section for proton elastic scattering from ^{48}Ca at 319 MeV.....46
5.2 Analyzing power for proton elastic scattering from ^{48}Ca at 319 MeV.....47
5.3 Differential cross-section for M1 transition in ^{48}Ca (p,p')$^{48}Ca^*$ at 319 MeV.....48
5.4 Analyzing power for M1 transition in ^{48}Ca (p,p')$^{48}Ca^*$ at 319 MeV.....49

5.5 Differential cross-section for proton elastic scattering from ^{48}Ca at 400 MeV....50
5.6 Analyzing power for proton elastic scattering from ^{48}Ca at 400 MeV....51
5.7 Differential cross-section for M1 transition in ^{48}Ca (p,p')$^{48}Ca^*$ at 400 MeV....52
5.8 Analyzing power for M1 transition in ^{48}Ca (p,p')$^{48}Ca^*$ at 400 MeV....53
5.9 Differential cross-section for proton elastic scattering from ^{48}Ca at 250 MeV....54
5.10 Analyzing power for proton elastic scattering from ^{48}Ca at 250 MeV....55
5.11 Differential cross-section for M1 transition in ^{48}Ca (p,p')$^{48}Ca^*$ at 250 MeV....56
5.12 Analyzing power for M1 transition in ^{48}Ca (p,p')$^{48}Ca^*$ at 250 MeV....57
5.13 Differential cross-section for proton elastic scattering from ^{48}Ca at 500 MeV....58
5.14 Analyzing power for proton elastic scattering from ^{48}Ca at 500 MeV....59
5.15 Differential cross-section for M1 transition in ^{48}Ca (p,p')$^{48}Ca^*$ at 500 MeV....60
5.16 Analyzing power for M1 transition in ^{48}Ca (p,p')$^{48}Ca^*$ at 500 MeV....61

1. Introduction

The study of nucleon-nucleus scattering at intermediate energies can be used to extract information about both the structure of the nucleus and the effective nucleon-nucleon (NN) interaction between nucleons in the nuclear medium.

An inelastic scattering reaction in which a nucleus is excited from an initial state $|\xi_i>$ to some final state $|\xi_f>$ may be described by a transition matrix (T). The matrix element for this process is directly related to the inelastic differential cross-section

$$(d\sigma/d\Omega) \alpha |<f|T|i>|^2, \qquad (1.1)$$

where the initial and final states of the scattering system, $|i>$ and $|f>$, belong to the product space of the projectile scattering states and the internal nuclear states $|\xi_i>$ and $|\xi_f>$. Measurement of the inelastic differential cross-section provides information about either the structure of the nucleus or the transition matrix for the process.

In the specific case of proton inelastic scattering, the transition between nuclear states is caused by the effective NN interaction between the incoming proton and one of the nucleons in the target nucleus. This interaction may be written [1] as a potential of the form

$$V_{eff} = V_o(r) + V_\sigma(r)\sigma_1\cdot\sigma_2 + V_\tau(r)\tau_1\cdot\tau_2 + V_{\sigma\tau}(r)\sigma_1\cdot\sigma_2\tau_1\cdot\tau_2 + [V_{LS}(r)+V_{LS\tau}(r)\tau_1\cdot\tau_2]\mathbf{L}\cdot\mathbf{S} + [V_T(r)+V_{T\tau}(r)\tau_1\cdot\tau_2]S_{12} \ . \qquad (1.2)$$

where σ and τ denote spin and isospin respectively, $\mathbf{L}\cdot\mathbf{S}$ is the usual spin-orbit operator and S_{12} is the tensor operator given by

$$S_{12} = 3(\sigma_1\cdot\hat{r})(\sigma_2\cdot\hat{r}) - \sigma_1\cdot\sigma_2 . \qquad (1.3)$$

The transition matrix element for a transition excited by proton inelastic scattering between two known nuclear states can be used to test the effective NN interaction in the nuclear medium.

A transition between two nuclear states may be described in terms of the angular momentum and parity changes that take place as a result of the excitation. In particular, a magnetic dipole (M1) transition requires that the two nuclear states differ by one unit of total angular momentum and have the same parity. It is known [1] that $V_{\sigma\tau}$ is the

largest term, by more than one order of magnitude, in the effective NN interaction which may excite an M1 transition from a $J^{\pi}=0^{+}$ ground state at low momentum transfer. Measurement of the differential cross-section for such a process can be used to obtain information about the $V_{\sigma\tau}$ term in the effective NN interaction provided that the initial and final states of the nucleus are understood.

The states of a nucleus may be described in terms of the independent particle model (IPM), where each nucleon is assumed to move independently in an average spherically symmetric potential. This gives rise to an energy level scheme characterized by a radial quantum number (n) and an orbital angular momentum quantum number (l). The nucleonic spin and orbital angular momentum combine to form a doublet state of total angular momentum $j=l\pm1/2$. When spin-orbit coupling is included, the degeneracies of the spin-orbit doublets are lifted, as illustrated in figure (1.1). Each state of total angular momentum (j) can accommodate (2j+1) protons and (2j+1) neutrons.

In general, the parity of an orbital angular momentum state is given by $\pi=(-1)^{l}$ so that a single particle transition from a $j=l+1/2$ level to its $j=l-1/2$ partner will obey the M1 selection rules. In terms of the independent particle model, M1 transitions in nuclei with filled $j=l+1/2$ levels and empty $j=l-1/2$ levels such as ^{12}C, ^{28}Si, ^{48}Ca, ^{90}Zr and ^{208}Pb arise from a single-particle transition to a single-particle single-hole configuration.

A strong M1 transition from the $J^{\pi}=0^{+}$ ground state of ^{48}Ca to a $J^{\pi}=1^{+}$ excited state at 10.23 MeV was first observed with inelastic electron scattering [2]. Since then, the excitation of this state with inelastic proton scattering has been studied extensively [3-8] at energies ranging from 44 to 334 MeV. The common feature of all of these studies is the large reduction or quenching of the observed M1 strength compared to that predicted by the independent particle model. The IPM overestimates the observed differential cross-section by a factor of three to four.

Two possible explanations for the quenching of the M1 strength have been proposed [9]. In one model [10], it has been suggested that the quenching arises from configuration mixing of the ^{48}Ca levels. In the independent particle model, the M1 transition results from a pure neutron transition from the filled $f_{7/2}$ to the empty $f_{5/2}$ shell with a completely inert closed $s_{1/2}$ proton shell. With configuration mixing, the 8 neutrons which occupy the filled $f_{7/2}$ shell are allowed to distribute over the complete $f_{7/2}\ f_{5/2}\ p_{3/2}\ p_{1/2}$ orbit space and couple to form many states with $J^{\pi}=1^{+}$, so that the M1 transition strength becomes fragmented. The fragmented strength is either shifted to higher excitation energies or spread out and made indistinguishable from the

background, quenching the IPM M1 strength. This quenching mechanism is discussed in detail in section (2.3c). It was found [10] that configuration mixing could account for only 25% of the observed quenching. Similarly, the effect of proton configuration mixing in the $d_{3/2}\, f_{7/2}\, f_{5/2}$ orbit space, originally believed to be negligible [11], gives rise to a further 10% quenching of the IPM estimate [12].

In the other picture [13], one of the target nucleons is excited into a Δ-nucleon hole state so that some of the M1 strength is shifted to very high excitation energies, as described in section (2.3d).

It is believed [13] that all of the missing M1 transition strength can be accounted for using a combination of both of these quenching mechanisms.

This work involves the measurement of the differential cross-section and the analyzing power of the M1 transition excited in the ^{48}Ca (p,p')$^{48}Ca^*$ reaction at incident beam energies of 250, 319 400 and 500 MeV. The experiment was carried out at the TRIUMF facility using the Medium Resolution Spectrometer (MRS) to examine the 10.23 MeV ($J^{\pi}=1^+$) state.

The measured differential cross-sections of the M1 transition were compared with the predictions of the independent particle model to establish the energy dependence of the quenching of the M1 transition strength in ^{48}Ca.

If extended calculations which account for the quenching mechanism can reproduce the data, the experimental cross-sections will give a direct measurement of the isovector spin-dependent central part of the effective nucleon-nucleon interaction $V_{\sigma\tau}$ in the nuclear medium.

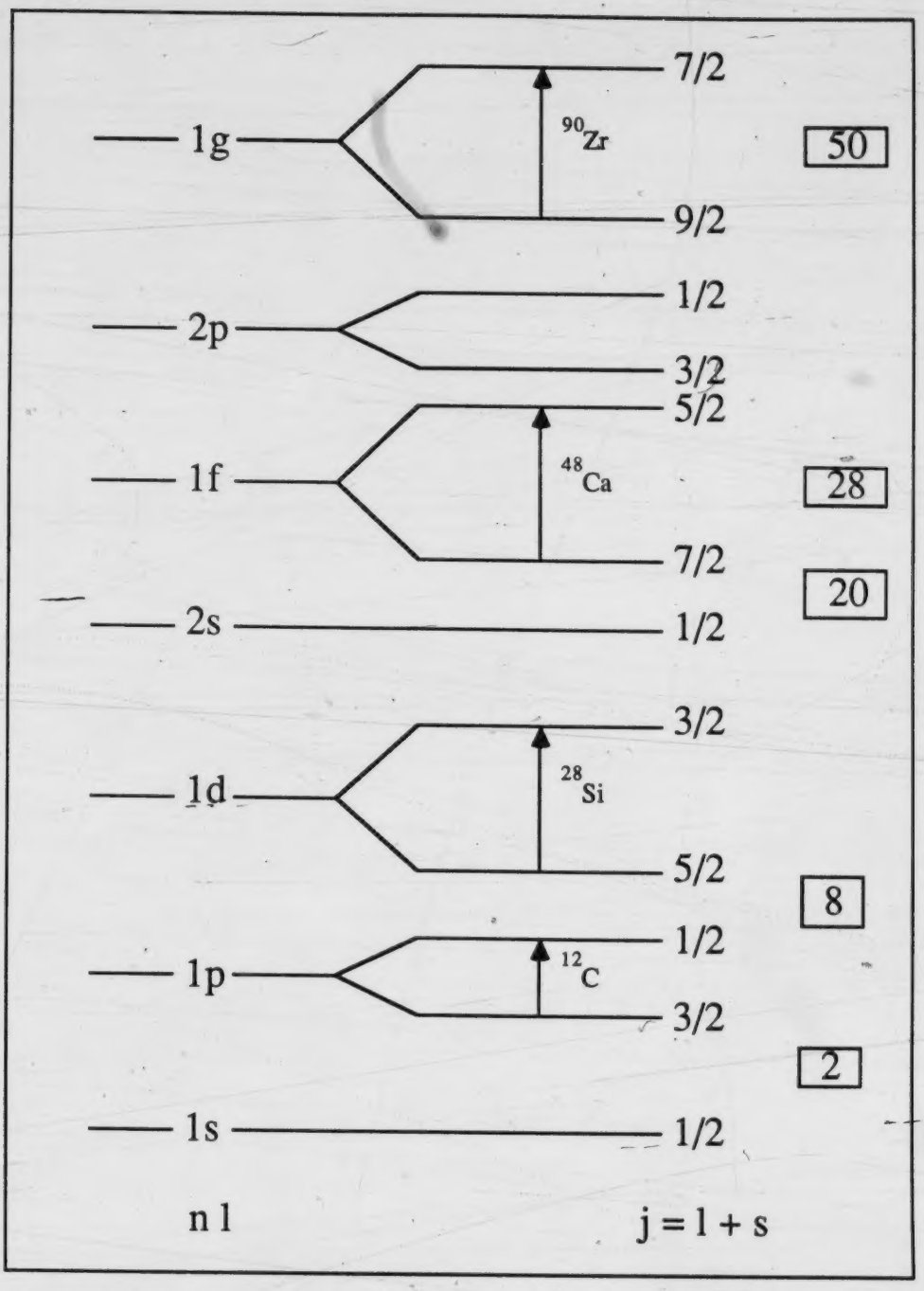

Figure 1.1 Order of nuclear energy levels according to the independent particle model. The boxes at the right of the figure indicate the number of nucleons which may be accomodated below the closed shell. M1 transitions to single-particle single-hole configurations are illustrated by the arrows.

2. Theory

2.1 Calculation of Scattering Observables

A scattering system which is excited from an initial state $|i>$ to a final state $|f>$ is described completely by the transition matrix element defined formally in equation (A1.10). Knowledge of the transition matrix element,

$$T_{fi} = \langle f | T | i \rangle \, , \qquad (2.1)$$

permits calculation of scattering observables such as the differential cross-section and analyzing power.

The differential cross-section of a nucleon-nucleus scattering reaction is given by

$$(d\sigma/d\Omega) = (\mu/2\pi\hbar^2)^2 (k'/k) ((2I+1) / 2) \sum | \langle f | T | i \rangle |^2 \, , \qquad (2.2)$$

where the sum is taken over all of the spin projections of both the incident nucleon and the spin-I target nucleus. The initial and final relative momenta of the nucleon-nucleus system are denoted by k and k' respectively and μ represents the reduced mass of the system.

The analyzing power is given by

$$A = Tr (T_{fi} \, \sigma \cdot n \, T_{fi}^{\dagger}) / Tr (T_{fi} \, T_{fi}^{\dagger}) \, , \qquad (2.3)$$

where **n** is a unit vector in the direction of **kxk'** and the trace is taken over the spin projections of the target nucleus and the incident nucleon.

With this description of nucleon-nucleus scattering, the problem of calculating any scattering observable reduces to the calculation of the transition matrix element for the process.

2.2 Calculation of the Transition Matrix Element (T_{fi})

The nucleon-nucleus scattering process is governed by the effective NN interaction between the incoming nucleon and the target nucleon within the nucleus. The transition matrix element describing an inelastic scattering reaction may be determined

from the NN interaction (V) using the formal scattering theory shown in appendix (1). The transition matrix element is given by equation (A1.13) as

$$T_{fi} = < \phi_f \xi_f | V | \Psi_i^+ \xi_i >, \qquad (2.4)$$

where $| \Psi_i^+ >$ represents an outgoing spherical wave in the initial channel and $| \phi_f >$ is a plane wave in the final channel. The initial and final states of the nucleus, $| \xi_i >$ and $| \xi_f >$, may be described in terms of some nuclear model such as the independent particle model.

Usually, actual calculations of the transition matrix element are carried out in the framework of some approximation scheme such as the Distorted Wave Born Approximation (DWBA) or the Distorted Wave Impulse Approximation (DWIA) which are shown in appendix (2).

2.2a Calculation of T_{fi} using the DWIA

The DWIA is based on the assumption that during a nucleon-nucleus scattering process, the incident nucleon interacts with only one target nucleon at a time. With this assumption,the effective NN interaction for nucleons within the nuclear medium can be replaced with the free NN interaction. The DWIA is valid only when the energy of the incident particles is greater than 100 MeV where the effect of multi-step processes is minimized.

The transition matrix element for an inelastic nucleon-nucleus scattering reaction is given in the DWIA by equation (A2.14) as

$$T_{fi} = < \chi_f^- \xi_f | \sum_j t_j^o | \chi_i^+ \xi_i > . \qquad (2.5)$$

The $| \chi^{\pm} >$ states represent the incoming and outgoing nucleon plane waves distorted by the optical potential, which describes the nucleon-nucleus elastic scattering reaction, as constrained by elastic scattering data. The free transition operator t_j^o describes the scattering of the incident nucleon by the jth target nucleon.

In previous analyses[7,8], the M1 transition strength in the ^{48}Ca (p,p')$^{48}Ca^*$ was calculated using the DWIA. The free transition operator was taken to be the Love-Franey interaction [1] which represents the free NN interaction as deduced from measurements of NN scattering observables. The intrinsic nuclear states, $| \xi_i >$ and

$|\xi_f>$, were calculated from the independent particle model.

2.2b Calculation of T_{fi} using the Density Dependent Interaction

Instead of assuming that the target nucleons behave independently during a scattering reaction, it is possible to take into account some of the effect of the nuclear medium on the incident nucleon. To accomplish this, the effective interaction between the incoming nucleon and the target nucleon is taken to depend on the position of the target nucleon within the nucleus [14]. Nuclear medium effects such as Pauli blocking begin to become important at incident energies below 500 MeV.

In accordance with the Pauli exclusion principle, the scattering problem must be solved subject to the restriction that the scattering states are not already occupied by any of the other nucleons in the nucleus.

A NN scattering reaction may be described by the transition matrix defined in equation (A1.11) as

$$T^{\pm} = V + V\, G_o^{\pm}\, T^{\pm} , \qquad (2.6)$$

where

$$G_o^{\pm} = (E - H_o \pm i\varepsilon)^{-1} . \qquad (2.7)$$

This may be recast into a form known as the Bethe-Goldstone equation,

$$T^{\pm}_{BG} = V + V\, G^{\pm}_{Q}\, T^{\pm}_{BG} , \qquad (2.8)$$

to describe the NN scattering process within the nuclear medium. The operator

$$G^{\pm}_{Q} = (E - H_o \pm i\varepsilon)^{-1}\, Q \qquad (2.9)$$

includes the medium effects by allowing for propagation only in unoccupied intermediate states which are projected out by the Pauli projection operator Q.

The general solution of the scattering problem is given by the Lipmann-Schwinger equation (A1.5) which is written in the Bethe-Goldstone form as

$$| \Psi^{\pm} > = | \phi > + G_Q^{\pm} V | \Psi^{\pm} > . \qquad (2.10)$$

By solving equation (2.10), it is possible to generate a complex energy and density dependent two-nucleon effective potential t(r). This density dependent interaction can be used to determine the transition matrix element for an inelastic scattering reaction.

The actual calculations of the transition matrix element are carried out using the DWBA which is given by equation (A2.5) as

$$T_{fi} = < \chi_f^- \xi_f | t(r) | \chi_i^+ \xi_i > . \qquad (2.11)$$

The distorted waves $| \chi^{\pm} >$ are calculated by solving the Schrödinger equation for an optical potential generated from the solution of equation (2.8).

The NN potential V is usually taken to be the semi-phenomenological Paris potential, which currently provides the most realistic description of the NN interaction. The Paris potential describes the long and medium range NN interaction by the exchange of one pion, two pions and the ω-meson between the interacting nucleons. At short range, where the internucleon distance is less than 0.8 fermis, the long and medium range description is replaced by a phenomenological soft core repulsive interaction.

Calculations for the ^{48}Ca (p,p')$^{48}Ca^*$ reaction were carried out at the University of Alberta using the DWBA83 code [15]. The initial and final states of the ^{48}Ca nucleus were taken as independent particle model wave functions from a harmonic oscillator basis set. The calculations represent a fully microscopic calculation of the transition matrix element from first principles with no adjustable parameters.

2.3 Quenching Mechanisms

Two different mechanisms have been proposed [9] to explain the quenching of the observed M1 strength compared to that expected from the independent particle model. These quenching mechanisms arise from deficiencies in the IPM description of the nucleus.

2.3a The Independent Particle Model (IPM)

A nucleus may be described as an assembly of nucleons with the Hamiltonian

$$H = \sum_i T_i + \sum_{i<j} V_{ij} . \qquad (2.12)$$

The kinetic energy operator T_i is summed over all nucleons and the potential energy V_{ij} is the interaction between the ith and jth nucleons summed over all pairs of nucleons.

Since it is impossible to obtain a description of the nucleus by solving the many body Schrödinger equation with the Hamiltonian from equation (2.12), simpler models of the nucleus must be introduced to permit nuclear structure calculations.

In the IPM, each nucleon is assumed to move independently in an average one-body potential u_i which describes the net potential due to the presence of the other nucleons in the nucleus. By adding and subtracting the single particle potential, equation (2.12) becomes

$$H = \sum_i (T_i + u_i) + \sum_{i<j} V_{ij} - \sum_i u_i . \qquad (2.13)$$

To simplify the notation, equation (2.13) may be written as

$$H = \sum_i h_i + V_R , \qquad (2.14)$$

where $h_i = T_i + u_i$ represents the Hamiltonian of a single independent particle in the average potential u_i.

By definition, the residual interaction

$$V_R \equiv \sum_{i<j} V_{ij} - \sum_i u_i \qquad (2.15)$$

repesents the difference between the two-body and one-body potentials.

In the pure IPM, the residual interaction is neglected and the nucleus is considered as an assembly of non-interacting particles. The independent particles obey the Schrödinger equation

$$h_i \mid \phi_n(i) > = E_n(i) \mid \phi_n(i) > , \qquad (2.16)$$

where the independent particle states $\mid \phi_n(i) >$ are usually taken from a harmonic oscillator basis set. The IPM wave function of the nucleus may be written as the antisymmetrized product of the independent particle states, giving rise to the energy level scheme illustrated in figure (1.1).

2.3b Transitions in a 3-Level System

Consider a 3-level quantum mechanical system in which an interaction Hamiltonian H causes transitions from the ground state $|0>$ to the excited states $|1>$ and $|2>$, with transition probabilities P_1 and P_2 respectively. In the presence of a perturbing potential V, the levels will be shifted so that new transition probabilities P_1' and P_2' will result, as illustrated in figure (2.1).

The energy E_n and eigenstate $|n>$ of any perturbed level are given by first order perturbation theory as

$$E_n = E_n^{\circ} + \langle n^{\circ} | V | n^{\circ} \rangle \qquad (2.17)$$

and

$$|n> = |n^{\circ}> + \sum_{j \neq n} (E_n^{\circ} - E_j^{\circ})^{-1} |j^{\circ}> \langle j^{\circ} | V | n^{\circ} > , \qquad (2.18)$$

in terms of the unperturbed states $|n^{\circ}>$ and the unperturbed energies E_n° .

For simplicity, it is assumed that only the two excited states, $|1>$ and $|2>$, are perturbed appreciably by the potential to become

$$E_1 = E_1^{\circ} + \langle 1 | V | 1 \rangle \qquad (2.19)$$

and

$$E_2 = E_2^{\circ} + \langle 2 | V | 2 \rangle . \qquad (2.20)$$

The perturbed states

$$|\Psi_1> = |1> + (E_1^{\circ} - E_2^{\circ})^{-1} |2> \langle 2 | V | 1 > \qquad (2.21)$$

and

$$|\Psi_2> = |2> + (E_2^{\circ} - E_1^{\circ})^{-1} |1> \langle 1 | V | 2 > \qquad (2.22)$$

may be written more simply as

$$|\Psi_1> = a|1> + b|2> \qquad (2.23)$$

and

$$|\Psi_2> = a|2> - b|1> . \qquad (2.24)$$

Equations (2.23) and (2.24) reveal that the effect of the perturbation is to mix the

states | 1 > and | 2 >.

The two perturbed states are orthonormal, requiring that

$$< \Psi_1 | \Psi_1 > = < \Psi_2 | \Psi_2 > = 1 \qquad (2.25)$$

and

$$< \Psi_1 | \Psi_2 > = 0 , \qquad (2.26)$$

which lead to

$$| a |^2 + | b |^2 = 1 \qquad (2.27)$$

and

$$a^* b = b^* a \qquad (2.28)$$

respectively.

The transition probabilities, in the absence of the perturbation, are given by

$$P_1 = | < 1 | H | 0 > |^2 \qquad (2.29)$$

and

$$P_2 = | < 2 | H | 0 > |^2 . \qquad (2.30)$$

In the presence of the perturbation, these become

$$P_1' = | < \Psi_1 | H | 0 > |^2 \qquad (2.31)$$

and

$$P_2' = | < \Psi_2 | H | 0 > |^2 . \qquad (2.32)$$

By substituting for $< \Psi_1 |$ and $< \Psi_2 |$ from equations (2.23) and (2.24), the perturbed transition probabilities become

$$P_1' = | a^* < 1 | H | 0 > + b^* < 2 | H | 0 > |^2 \qquad (2.33)$$

and

$$P_2' = | a^* < 2 | H | 0 > - b^* < 1 | H | 0 > |^2 . \qquad (2.34)$$

Expanding and using the result of equation (2.28) that a*b is real, the changes in the transition probabilities, $\Delta P_i = P_i' - P_i$, caused by the perturbation are given by

$$\Delta P_1 = (|a|^2 - 1)|\langle 1|H|0\rangle|^2 + |b|^2|\langle 2|H|0\rangle|^2 + 2a^*b\ \mathrm{Re}(\langle 1|H|0\rangle\langle 2|H|0\rangle^*) \quad (2.35)$$

and $$\Delta P_2 = (|a|^2 - 1)|\langle 2|H|0\rangle|^2 + |b|^2|\langle 1|H|0\rangle|^2 - 2a^*b\ \mathrm{Re}(\langle 2|H|0\rangle\langle 1|H|0\rangle^*)\ . \quad (2.36)$$

If the perturbation is such that the degree of configuration mixing between states $|1\rangle$ and $|2\rangle$ is small, terms of the order $|b|^2$ may be ignored. Using equation (2.27), equations (2.35) and (2.36) reduce to

$$\Delta P_1 = 2a^*b\ \mathrm{Re}(\langle 1|H|0\rangle\langle 2|H|0\rangle^*) \quad (2.37)$$

and

$$\Delta P_2 = -2a^*b\ \mathrm{Re}(\langle 1|H|0\rangle\langle 2|H|0\rangle^*)\ . \quad (2.38)$$

In this picture, the perturbation transfers some of the transition probability between the unperturbed $|0\rangle \rightarrow |1\rangle$ and $|0\rangle \rightarrow |2\rangle$ transitions, as illustrated in figure (2.2).

2.3c Quenching due to Configuration Mixing

In the IPM, the structure of the ^{48}Ca nucleus is described by a closed $2s_{1/2}$ ^{40}Ca core with the additional 8 neutrons filling the $f_{7/2}$ level. The remaining $f_{5/2}$, $p_{3/2}$ and $p_{1/2}$ levels of the major shell are completely empty. The M1 transition is represented as a single neutron transition from the filled $f_{7/2}$ level to the empty $f_{5/2}$ level.

To provide an improved description of the ^{48}Ca nucleus, the residual interaction, defined by equation (2.15), may be treated as a perturbation to the independent particle states. The perturbation will mix the IPM states so that the 8 neutrons from the filled $f_{7/2}$ level will be distributed over the complete $f_{7/2}$ $f_{5/2}$ $p_{3/2}$ $p_{1/2}$ orbit space.

With configuration mixing, the IPM states will couple to form many states with $J^\pi=1^+$ which will be excited by an M1 transition. This will fragment some of the strength from the strong single transition in the IPM into many weaker transitions which may be indistinguishable from the background, as illustrated in figures (2.3a) and (2.3b). Furthermore, by applying the model described in chapter (2.3b), with the ground state of the ^{48}Ca nucleus ($J^\pi=0^+$)represented by the $|0\rangle$ state and both $|1\rangle$ and $|2\rangle$ representing $J^\pi=1^+$ states, some of the transition strength may be transferred between the

various M1 transitions. This results in further quenching of the IPM strength, as illustrated in figure (2.3c).

In this model, the excitation energy for the M1 transition is the sum of the single-particle single-hole configuration energy of the IPM and the energy of the residual interaction, given by equations (2.19) and (2.20). Measurement of the excitation energy and comparison to the IPM estimate can be used to obtain information about the particle-hole residual interaction.

A calculation of the M1 transition strength in the ^{48}Ca (p,p')$^{48}Ca^*$ has been performed by McGrory and Wildenthal [10]. It was found that the M1 strength was dominated by the $f_{7/2} \rightarrow f_{5/2}$ transition and that configuration mixing reduced the M1 strength by 25% from the IPM prediction.

2.3d Δ-Nucleon Hole Quenching Mechanism

The $V_{\sigma\tau}$ term in the effective NN interaction which is responsible for the M1 transition can also excite the target nucleon into a Δ-nucleon hole state [9].

The mechanism of Δ-nucleon hole quenching can be understood by applying the 3-level model described in chapter (2.3b), with the ground state of the ^{48}Ca nucleus ($J^\pi=0^+$) represented by $|0>$, the $J^\pi=1^+$ state by $|1>$ and the Δ-nucleon hole state by $|2>$. If the $a^*b\,Re(<1|H|0><2|H|0>^*)$ term which appears in equations (2.37) and (2.38) is negative, then part of the M1 strength will be transfered to the Δ-nucleon hole transition which lies at an excitation energy of 300 MeV, quenching the IPM M1 strength.

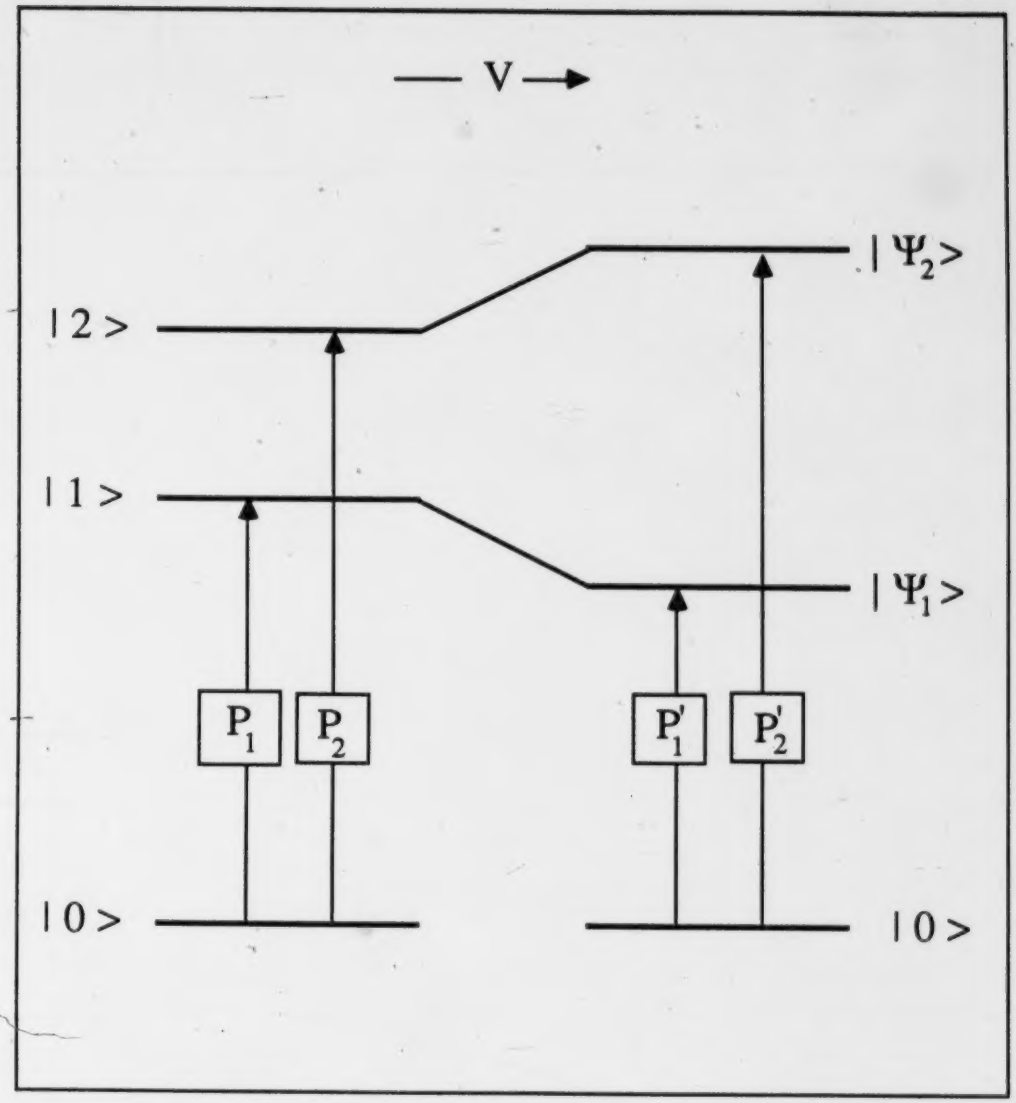

Figure 2.1 The effect of a perturbation V on transitions in a 3-level system.

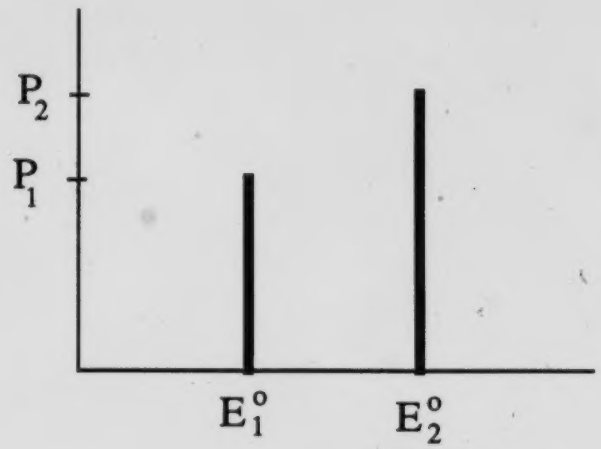

Figure 2.2a Excitation energy spectrum of unperturbed 3-level system.

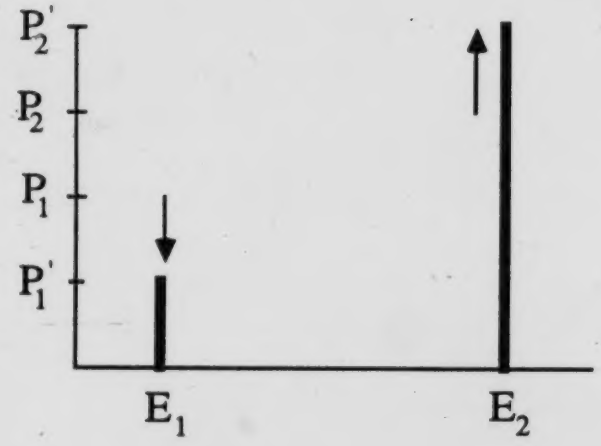

Figure 2.2b Excitation energy spectrum of 3-level system after perturbation.

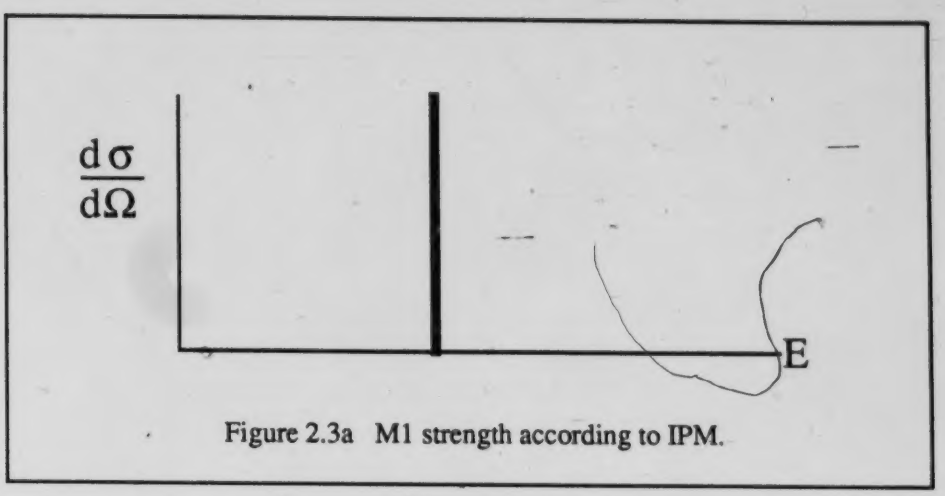

Figure 2.3a M1 strength according to IPM.

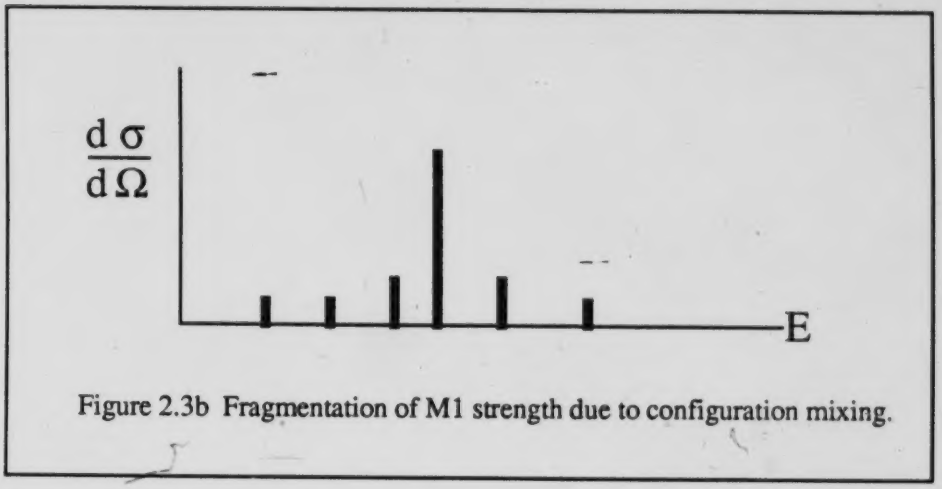

Figure 2.3b Fragmentation of M1 strength due to configuration mixing.

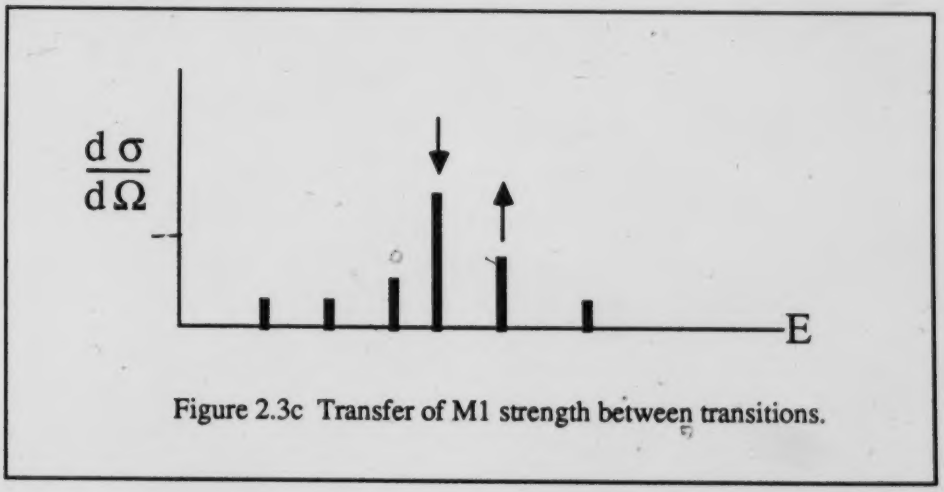

Figure 2.3c Transfer of M1 strength between transitions.

3. Experimental Arrangement

3.1 General Description

The TRIUMF cyclotron is capable of delivering a proton beam with an energy of up to 500 MeV. The beam is produced by accelerating H^- ions injected from the ion source and extracted by means of a carbon stripper foil which strips the electrons from each ion causing the resulting proton to leave the cyclotron. By adjusting the radial position of the stripper foil, the beam energy may be varied continuously from 200 to 500 MeV. The beam is bunched in packets 1 to 4 nanoseconds wide coming every 43 nanoseconds, and may be polarized up to 80% at an intensity of 600 nanoamperes or unpolarized with an intensity up to 150 microamperes.

The general layout of the TRIUMF facility is presented in figure (3.1). The $^{48}Ca\ (p,p')^{48}Ca^*$ experiment was performed on beam line 4B (BL4B) in the Proton Hall experimental area using the Medium Resolution Spectrometer (MRS), which is illustrated in figure (3.2).

3.2 The Medium Resolution Spectrometer (MRS)

The MRS is a large energy-loss spectrometer which may be rotated about the target in the scattering plane to measure the energy of a proton after scattering through some angle at the target. The spectrometer consists of a quadrupole and a dipole magnet together with a series of multiwire chambers required to reconstruct a particle's path through the MRS. The coordinate-system of the MRS, defined relative to the central trajectory through the spectrometer, is illustrated in figure (3.3).

After scattering at the target, a particle passes through the Front-End-Chamber (FEC) which identifies the point of entry into the MRS and also serves, in conjunction with the top scintillators, as a trigger for the MRS electronics. The FEC is a standard 8cm x 8cm drift chamber which is made up of 2 orthogonal sets of 2 staggered planes each planes of 16wires, labelled as X_o and Y_o. It contains pure isobutane at 250 Torr and is capable of a maximum count rate of 1 MHz. The MRS may be set to accept an event when a particle is detected in either the (X_o or Y_o) plane or both (X_o and Y_o) planes. The solid angle acceptance of the MRS is ultimately determined by software cuts on the X_o and Y_o coordinates.

After acceptance into the spectrometer, the scattered protons are focussed in the

transverse Y-plane by the quadrupole magnet and momentum-analyzed by the large 60°-bend dipole magnet before passing through two Vertical-Drift-Chambers (VDC) located at the top of the MRS. The VDC's each contain 2 planes of 176 wires in 1 atmosphere of 50% isobutane and 50% argon to measure the position of a particle's trajectory, within fractions of a millimeter, in the dispersion plane X and U, a coordinate oriented at 30° to the X-axis from which the transverse Y-coordinate may be calculated. They are capable of a maximum count rate of approximately 10^5 per wire. The active area of each VDC is 115cm x 30cm, but this is effectively reduced by a factor of $\sqrt{2}$ since the chambers are oriented at an angle of 45° to the optic axis of the spectrometer. The coordinates measured by the lower and upper VDC's are denoted by X_1,U_1 and X_2,U_2 respectively.

Based on the geometry illustrated in figure (3.4), the VDC information is used to calculate the position,

$$X_F = [\, GS_1 - F\,(S_1 - S_2)\,] \,/\, [\, G - (S_1 - S_2)\tan\delta\,]\,, \qquad (3.1)$$

where a particle's trajectory intersects the focal plane, with $S_1 = X_1 + H$ and $S_2 = X_2$.

For ray tracing through the spectrometer, it is necessary to know the particle's trajectory as it crosses the VDC's. This may be specified in terms of the angles

$$\theta = (2G)^{-1}\,[\, G - H + (X_2 - X_1)\,] \qquad (3.2)$$

in the dispersion plane, as illustrated in figure (3.4), and similarly

$$\phi = (Y_2 - Y_1) \,/\, (G^2 + (S_1 - S_2)^2)^{1/2} \qquad (3.3)$$

in the transverse plane.

The VDC and FEC information may be used to reconstruct the path of the particle back to the target. The calculated coordinates,

$$X_I = a\,X_o + b\,\theta \qquad (3.4)$$

and

$$Y_I = c\,Y_o + d\,\phi\,, \qquad (3.5)$$

refer to the position of the particle at the target. To help reduce the background, the X_I

and Y_I coordinates may be constrained to require that any detected particle originate at the target within the beam spot.

Located in the dispersion plane at the top of the MRS, an array of 6mm thick by 10cm wide plastic scintillators ("paddles"), which measure a particle's energy loss as it passes through the scintillator, are used to select the momentum acceptance of the MRS and, in conjunction with the FEC trigger, to measure the time-of-flight through the spectrometer. This information is required to identify the type of particle which has been detected.

A veto scintillator paddle ("Elastic Prescaler") is available to prescale the number of events which are accepted from a certain region of the focal plane. This is necessary to supress strong peaks, such as the elastic scattering peak, which would otherwise make the study of weakly excited states impossible.

3.3 Dispersion Matching

To optimize the energy resolution of the MRS, it is necessary to decouple the energy-loss resolution of the spectrometer from the energy spread of the beam by using a technique known as dispersion matching.

In general, a proton beam with an energy $E \pm \Delta E$ which passes through a dipole magnet will be dispersed by an amount ΔX, depending upon the dispersion characteristics of the magnet, as illustrated in figure (3.5a).

The beam characteristically produced by the TRIUMF cyclotron is momentum dispersed in the horizontal plane, perpendicular to the dispersion plane of the MRS. If an MRS experiment was performed under these conditions, resolution of a state at some excitation energy E_x would be limited by the energy spread of the beam, as illustrated in figure (3.5b). Since the beam energy spread is typically 1 MeV or more, depending upon the beam tune, the resolution of excited nuclear states would be very limited in this mode of operation.

The principle of dispersion matching can be seen by reversing the trajectories of the protons illustrated in figure (3.5a). By orienting the dispersion plane of the beam to coincide with the dispersion plane of the spectrometer, all the protons in a beam with an energy spread of ΔE and dispersed by ΔX will focus to a single point on the focal plane.

In the MRS experiment, all protons which lose energy E_x in the target will intersect the focal plane of the spectrometer at the same point, regardless of the initial proton energy, as illustrated in figure (3.5c). In this dispersion matched mode of

operation, energy resolutions of 100-200 keV may be obtained.

To achieve dispersion matching, the horizontal momentum dispersion of the beam is rotated into the vertical plane by an assembly of 6 quadrupole magnets, collectively refered to as the TWISTER.

3.4 Beam Line 4B

The general layout of beam line 4B (BL4B) in the Proton Hall experimental area is presented in figure (3.6).

Located at the upstream end of beam line 4B, the In-Beam-Polarimeter (IBP) is used to continuously monitor both the polarization and the flux of the beam. The arrangement of the IBP is illustrated in figure (3.7) . It consists of a CH_2 target and a series of detectors made up of plastic scintillators and photomultiplier tubes. The detectors are positioned at scattering angles of 17^o and 70^o to detect the scattered and the recoil protons in coincidence. The polarization of the beam normal to the scattering plane is determined from the asymmetry in the number of counts between the left and right set of detectors. The beam flux is obtained from the total number of counts in the IBP. Some of the specifications of the IBP appropriate to ^{48}Ca (p,p')$^{48}Ca^*$ experiment are listed in appendix (3).

The TWISTER magnet assembly is located immediately downstream of the IBP.

The 14.37 mg cm^{-2} ^{48}Ca target was located in the scattering chamber at 4BT2. Since ^{48}Ca oxidizes very rapidly in the air, the target was stored under vacuum and transfered directly to the scattering chamber without exposing it to the atmosphere.

3.5 On-Line Analysis

Data from the MRS instrumentation is read by the Computer Automated Measurement and Control system (CAMAC) and passed to a Data General Eclipse computer located in the MRS counting room. All events are written onto magnetic tape before some portion of these are processed on-line by the Data Acquisition System (DACS).

The experimental coordinates are calculated by the DACS and spectra are histogrammed according to software cuts on the coordinates. DACS also allows scalers and scaler rates, such as those from the IBP, to be monitored.

A typical on-line spectrum taken during the ^{48}Ca (p,p')$^{48}Ca^*$ experiment

showing the number of counts as a function of focal plane position, which corresponds to an excitation energy spectrum of the ^{48}Ca nucleus is presented in figure (3.8). The large momentum acceptance of the MRS results in a large range of scattered proton energies to be distributed on the the focal plane. The largest peak occuring in channel 14200 corresponds to proton elastic scattering from ^{48}Ca. The first excited state of ^{48}Ca, with $J^{\pi}=2^{+}$ at an excitation energy of 3.83 MeV, is located in channel 14960. The strong M1 transition to the $J^{\pi}=1^{+}$ state at 10.23 MeV can be seen in channel 16300.

By replaying the magnetic tape data with more careful constraints on the coordinates, much of the background characteristic of on-line spectra can be eliminated. The addition of correction terms to the calculated coordinates improves the resolution of the focal plane spectrum.

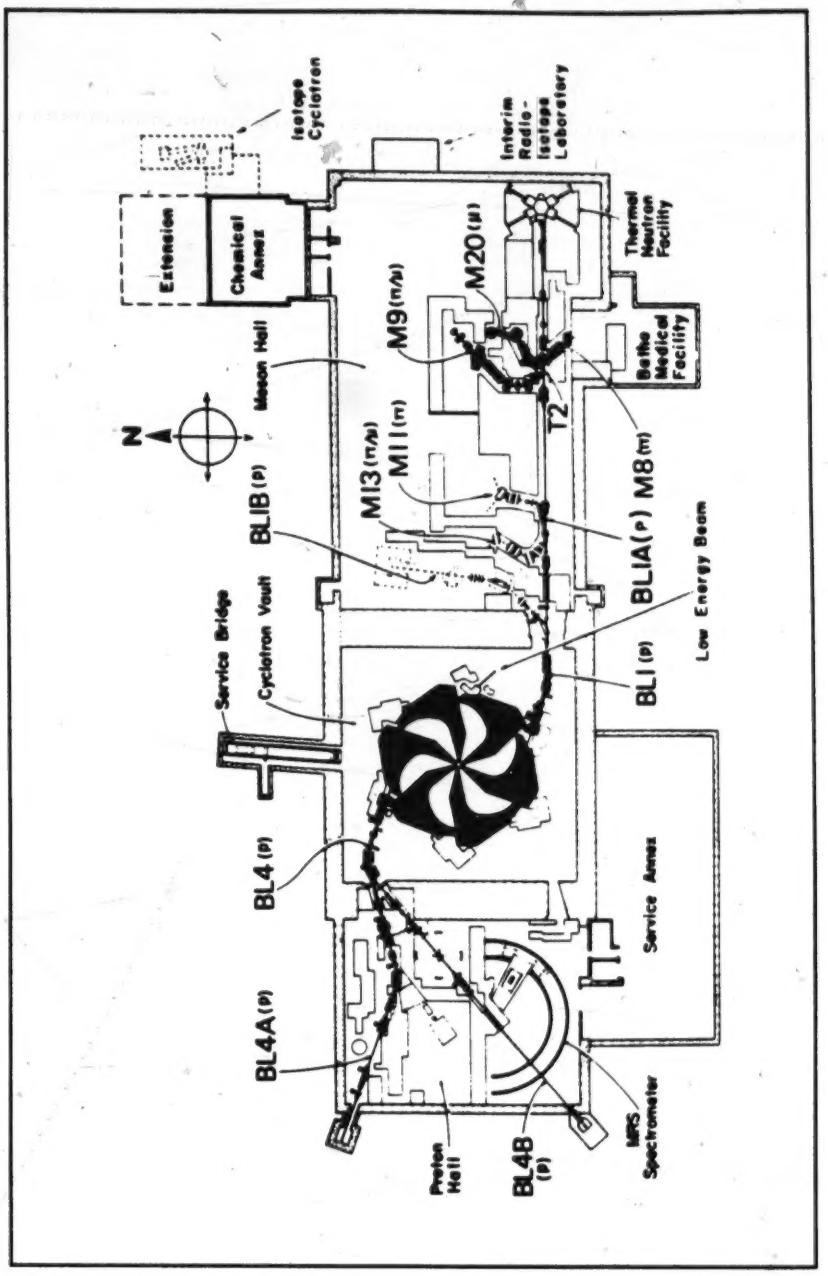

Figure 3.1 General layout of the TRIUMF facility.

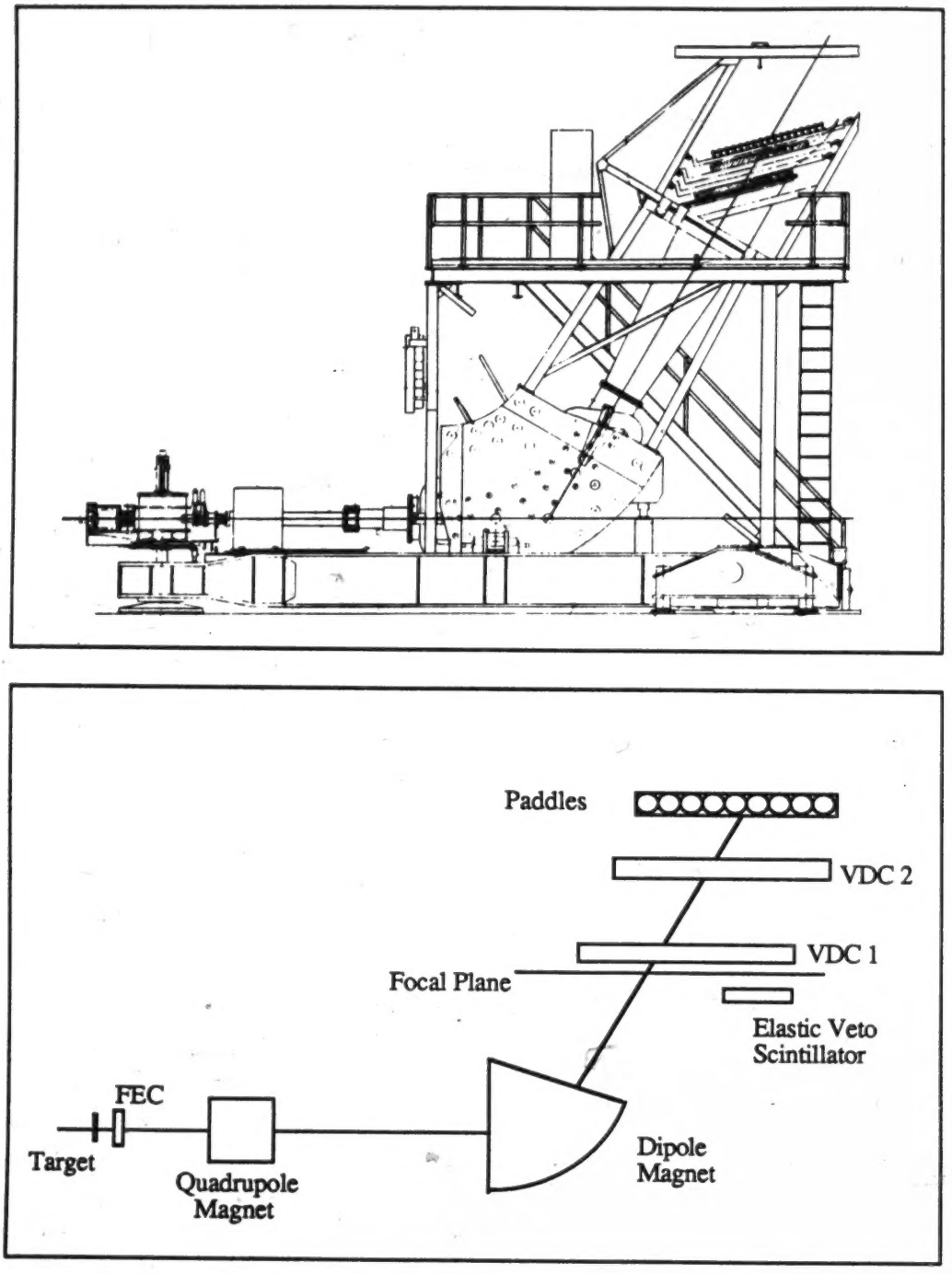

Figure 3.2 The Medium Resolution Spectrometer.

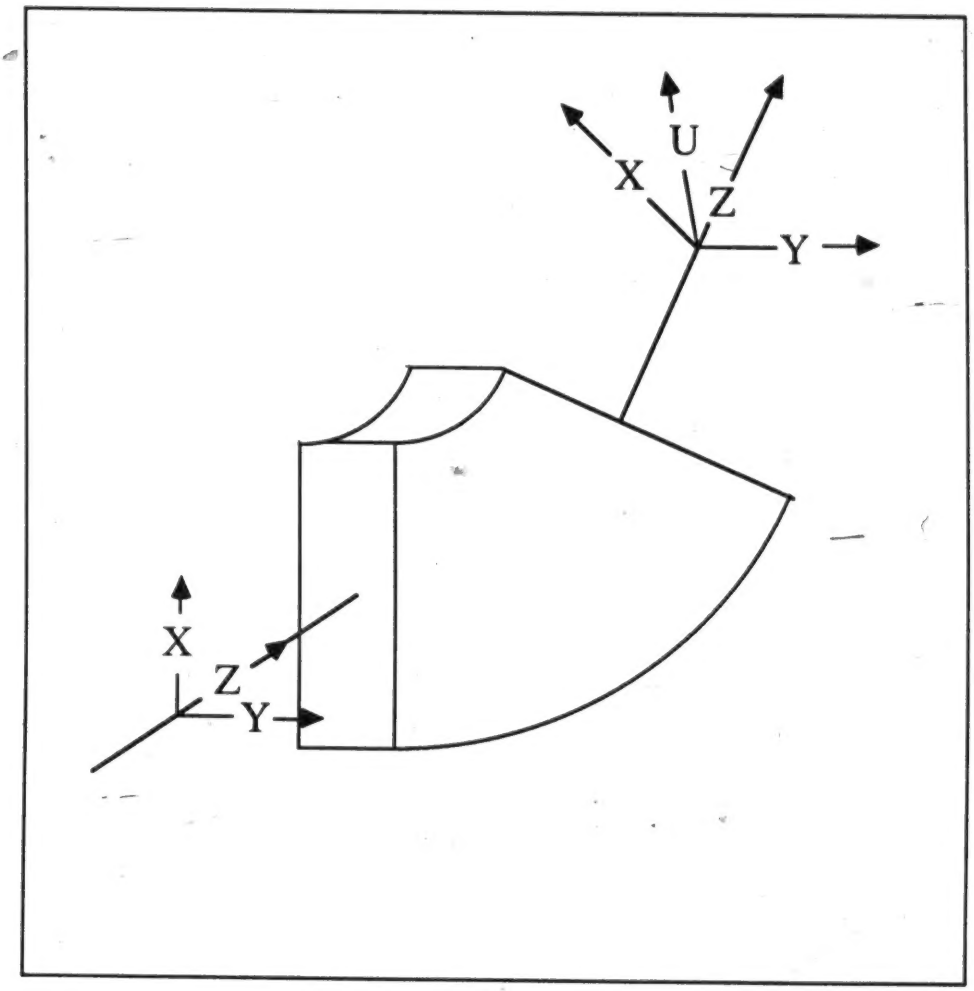

Figure 3.3 The MRS coordinate system.

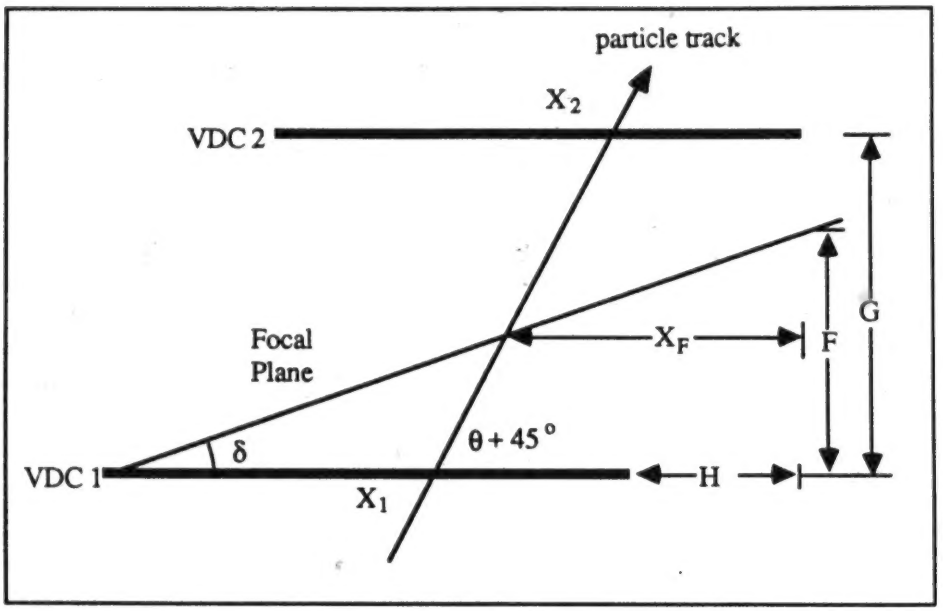

Figure 3.4 Geometry of the MRS focal plane.

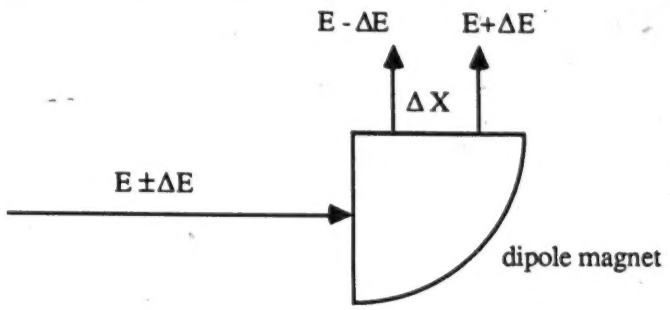

Figure 3.5a Dispersion of a proton beam by a dipole magnet.

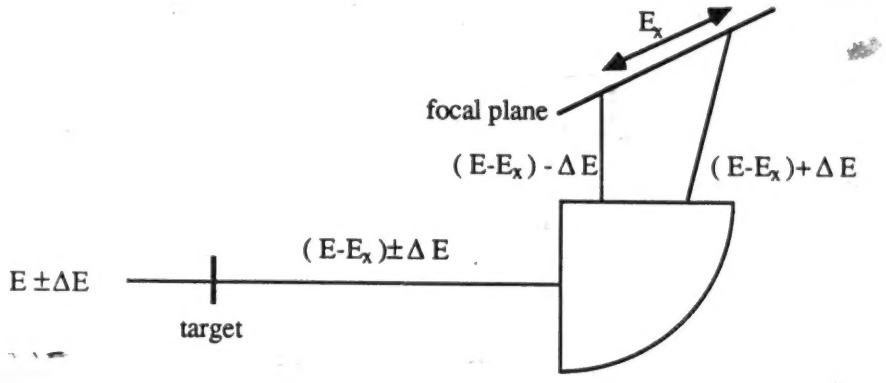

Figure 3.5b Operation of MRS with horizontal beam dispersion.

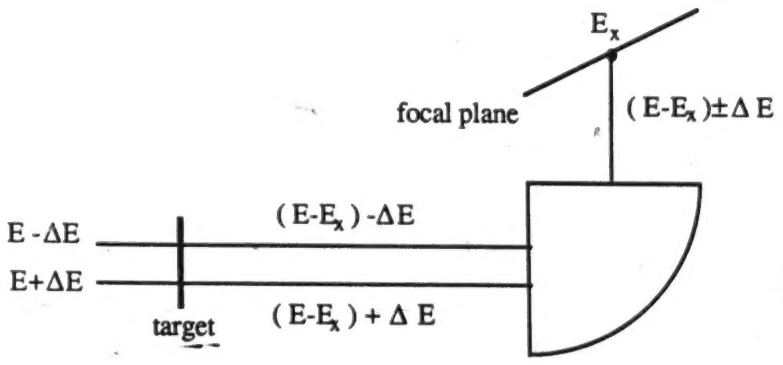

Figure 3.5c Operation of MRS with dispersion matching.

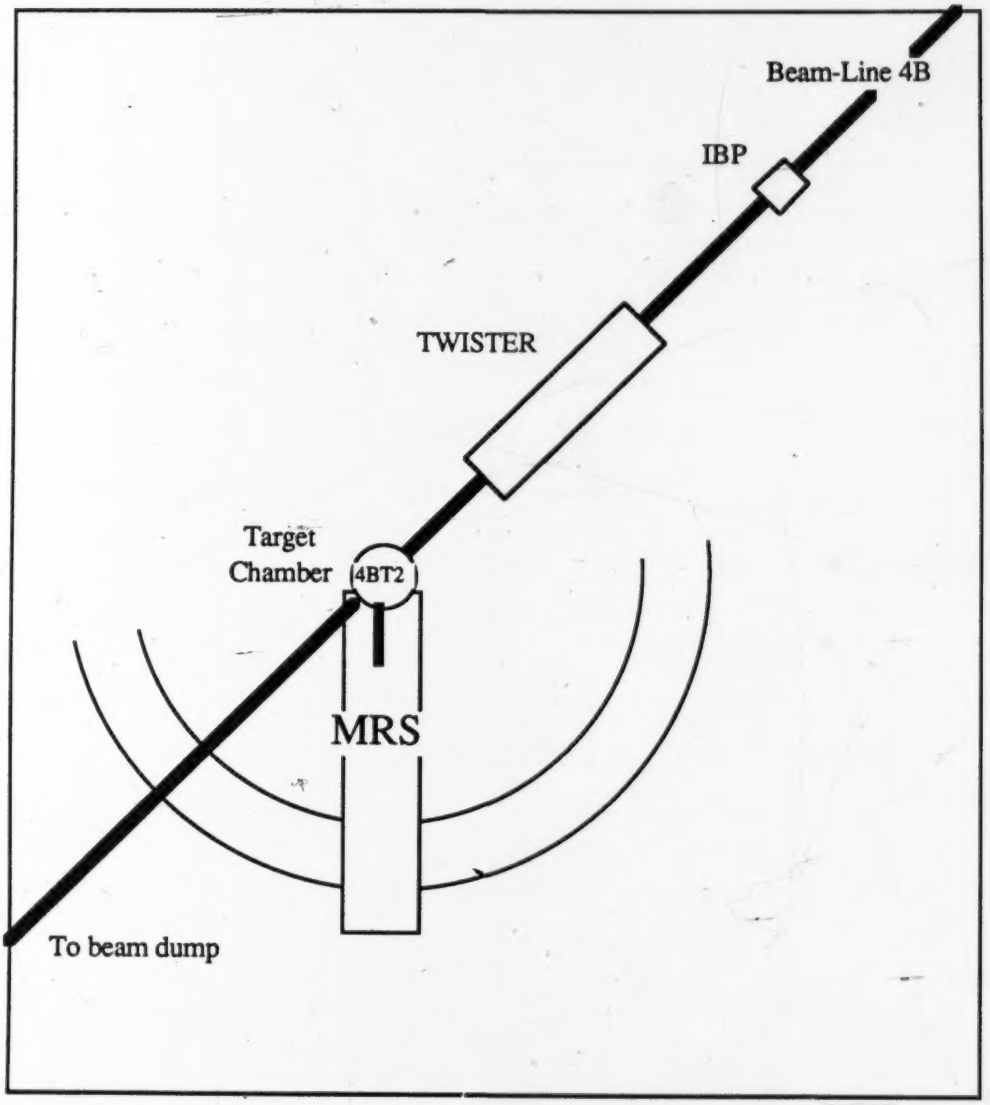

Figure 3.6 Proton Hall layout showing Beam Line 4B

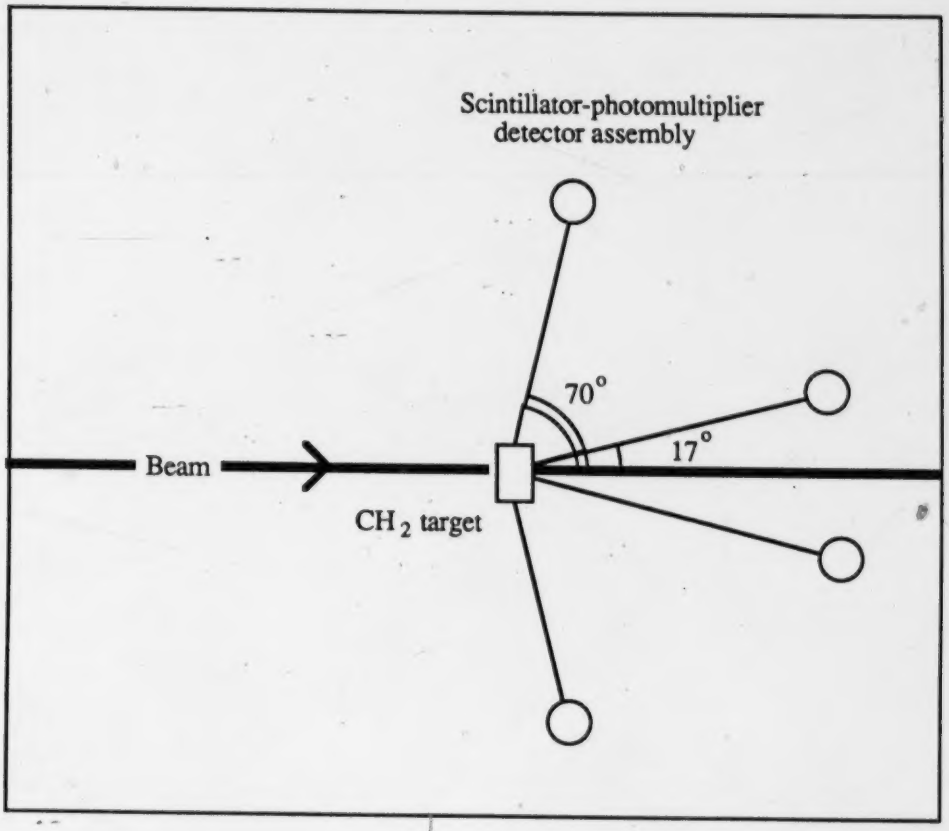

Figure 3.7 Arrangement of the In-Beam-Polarimeter (IBP)

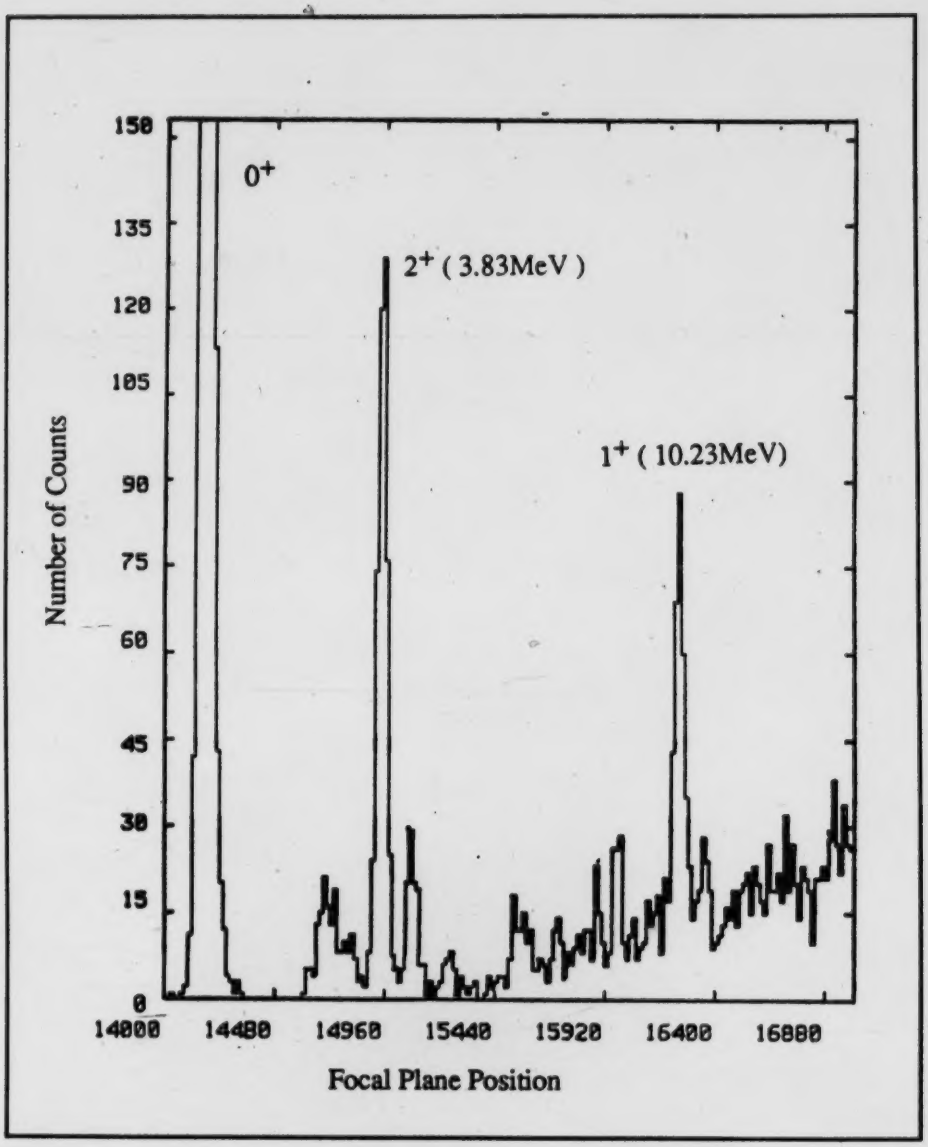

Figure 3.8 Typical on-line focal plane spectrum for the ^{48}Ca (p,p') ^{48}Ca* reaction.

4. Analysis

4.1 General Description

The focal plane spectrum, which corresponds to an excitation energy spectrum of the ^{48}Ca target nucleus, is used to determine the differential cross-section and analyzing power of the M1 transition excited in the ^{48}Ca (p,p')^{48}Ca* reaction.

The goal of the replay analysis is to produce a focal plane spectrum with an optimum energy resolution and a minimum amount of background events.

The MRS data, written onto magnetic tape by the DACS during the experiment, was replayed at the University of Alberta on a Digital Equipment Corporation VAX 780 computer using the LISA [16] data analysis program.

4.2 The LISA Data Analysis Program.

LISA is an interactive data analysis program designed to process event mode data from Nuclear Physics experiments. Although many of its features are completely general, the present implementation of LISA has been specifically tailored to process DACS written tapes from MRS experiments.

The LISA program processes each event according to the user-defined FORTRAN routine "INSERT" where new coordinates are generated and coordinate corrections are applied. LISA allows a variety of conditions to be defined which constrain the processing of events. A condition may be defined as a window on a coordinate, a two-dimensional window on a two-dimensional spectrum or a bit mask on a coordinate. Complex conditions may be constructed from logical expressions of conditions. During the processing of each event, conditions are tested and previously defined spectra are histogrammed according to specified conditions.

For a further description of the LISA program and the actual syntax of LISA commands, refer directly to the LISA documentation [16].

4.3 Replay Analysis

4.3a Coordinate Corrections

In the replay analysis, corrections are applied to the X_F and θ coordinates to

improve the resolution of the focal plane spectrum.

The θ coordinate depends on the momentum of the detected particle and is corrected, to make it momentum independent, according to its position on the focal plane using

$$\theta_{PC} = \theta + a X_F \ . \qquad (4.1)$$

By substituting θ_{PC} into equation (3.4), an improved the expression for X_I may be written as

$$X_I = a X_o + b \theta_{PC} \ . \qquad (4.2)$$

Several corrections must be applied to the focal plane position X_F to optimize the resolution of the focal plane spectrum.

The energies of protons scattered into the angular acceptance of the spectrometer are coupled to their respective scattering angles according to reaction kinematics. This so-called kinematic shift results in a loss of energy resolution of the spectrometer as demonstrated in appendix (5). To compensate for the kinematic shift effect, it is necessary to introduce a correction in Y_o to the focal plane position.

The remaining terms are intoduced as empirical corrections for geometric aberrations in the MRS optics and any dispersion mismatching.

The corrected focal plane position is given by

$$X_{FPC} = X_F + a \theta_{PC} + b (\theta_{PC})^2 + c (\theta_{PC})^3 + d (\theta_{PC})^4 + e (Y_o - e')$$

$$+ f (Y_o - f')^2 + g (X_o - g') + h (X_o - h')^2 + k \theta_{PC} (X_o - k') \ , \qquad (4.3)$$

where the coefficients of each of the correction terms are adjustible parameters chosen such that X_{FPC} is independent of the correction coordinates, as illustrated in figures (4.1) and (4.2). The optimum correction coefficients can be calculated automatically with the FFIT routine contained in the LISA software package. When the data is replayed with these corrections, the focal plane spectrum X_{FPC} is histogrammed with optimum resolution.

4.3b Background Reduction

It is possible to reduce the background which appears in the focal plane spectrum by excluding undesirable events from the analysis.

The first constraint placed on the acceptance of an event is that the particle must be detected by all of the MRS detectors.

Secondly, in the particular case of the ^{48}Ca (p,p')^{48}Ca* experiment, the detected particle must be identified as a proton based on the energy deposited in the paddles in conjunction with the time-of-flight through the spectrometer. This constraint will exclude accidentally triggered events as well as deuterons, tritons or pions which may be produced through some other nuclear reaction at the target.

It is also desirable to constrain the X_I and Y_I coordinates to ensure that a detected particle originate at the target. This cut is necessary to exclude events which originate from some other part of the target assembly or scatter in some part of the spectrometer. An image of the target assembly can be seen in the spectrum of Y_I versus X_I presented in figure (4.3). A cut must be placed around the centre of the image to include only protons scattered from the ^{48}Ca target.

It is important to ensure that constraints placed on any coordinate do not effectively cut the X_o or Y_o coordinates, which determine the solid angle acceptance of the spectrometer, and would lead to incorrectly calculated cross-sections.

4.3c Spectra

The X_{FPC} spectra are histogrammed subject to all of the desired constraints on the coordinates. A typical focal plane spectrum X_{FPC} for the ^{48}Ca (p,p')^{48}Ca* reaction is presented in figure (4.4).

Separate spectra may be defined to include gating with other conditions such as the UP / DOWN / OFF polarization state of the beam to measure polarization observables. It is also useful to gate the focal plane spectra with bins in Y_o to resolve one set of data into several angular bins.

The LISA software package provides background subtraction and gaussian fitting routines to obtain the number of counts in a given state.

4.3d Determination of Overall MRS Efficiency

When a particle passes through a set of detectors { A, B, C, D . . . }, the overall efficiency of the detector system ε is defined as the probability that the particle is detected by all of the detectors in the set. This may be determined from the individual detector efficiencies { $\varepsilon_A, \varepsilon_B, \varepsilon_C, \varepsilon_D \ldots$} using

$$\varepsilon = \varepsilon_A \, \varepsilon_B \, \varepsilon_C \, \varepsilon_D \ldots \qquad (4.4)$$

assuming that there are no correlations between the detector inefficiencies.

It is possible to determine an individual detector efficiency by calculating the probability that it detects a particle which is also detected by all of the other detectors in the set. For example, the efficiency of detector A is given by

$$\varepsilon_A = [\, A \times B \times C \times D \ldots] / [\, B \times C \times D \ldots], \qquad (4.5)$$

where x represents the logical "and" operation.

The overall efficiency of the MRS is given by

$$\varepsilon_{MRS} = \varepsilon_{FEC} \, \varepsilon_{X1} \, \varepsilon_{X2} \, \varepsilon_{U1} \, \varepsilon_{U2} \, . \qquad (4.6)$$

Following equation (4.5), the efficiency of the FEC for detecting protons is given by

$$\varepsilon_{FEC} = [\, X_o \times Y_o \times X_1 \times X_2 \times U_1 \times U_2 \times PROT\,] / [\, X_1 \times X_2 \times U_1 \times U_2 \times PROT\,], \qquad (4.7)$$

where PROT refers to the condition that the detected particle is identified as a proton. The efficiencies of the upper VDC's { ε_{X1} , ε_{X2} , ε_{U1} , ε_{U2} } may be calculated similarly.

During the data acquisition, it is necessary that the MRS trigger requirement be set to (X_o or Y_o) and assume that this will cause the MRS to trigger on all scattering events.

4.4 Calculation of Differential Cross-Section and Analyzing Power

The differential cross-section ($d\sigma/d\Omega$) for a scattering reaction, at a particular angle and incident energy, is determined from experiment with the relation

$$(d\sigma/d\Omega) = (N) / [(\text{livetime}) (\varepsilon_{MRS}) (d\Omega) (\text{target thickness}) (\text{flux})] . \quad (4.8)$$

N is the number of counts under the peak of interest in the focal plane spectrum, the target thickness is given in nuclei cm^{-2} (^{48}Ca thickness = 14.37 mg cm^{-2} = 1.803×10^{20} nuclei cm^{-2} in this experiment.) and the incident beam flux is determined from the IBP. The livetime of the MRS electronics is determined from the fraction of pulser generated events processed by the system. The solid angle acceptance of the MRS $d\Omega$ is calculated from the target-FEC geometry based on cuts on the X_o and Y_o coordinates.

The differential cross-section $(d\sigma/d\Omega)_p$ measured using a beam with polarization **P** depends on the analyzing power **A** of the target

$$(d\sigma/d\Omega)_p = (d\sigma/d\Omega)_o [1 + \mathbf{P} \cdot \mathbf{A}] , \quad (4.9)$$

where $(d\sigma/d\Omega)_o$ is the differential cross-section which would be measured using an unpolarized beam.

The values of $(d\sigma/d\Omega)_o$ and A can be determined by measuring $(d\sigma/d\Omega)_p$ for beams polarized normal to the scattering plane with polarization P^+ for the spin-up case and P^- for spin-down. Using equation (4.9) it is possible to write

$$(d\sigma/d\Omega)_+ = (d\sigma/d\Omega)_o [1 + P^+A] \quad (4.10)$$

and $$(d\sigma/d\Omega)_- = (d\sigma/d\Omega)_o [1 - P^-A] \quad (4.11)$$

for the spin-up and spin-down cases respectively. Solving these equations for $(d\sigma/d\Omega)_o$ and A yields

$$(d\sigma/d\Omega)_o = [P^-(d\sigma/d\Omega)_+ + P^+(d\sigma/d\Omega)_-] / [P^+ + P^-] \quad (4.12)$$

and $$A = [(d\sigma/d\Omega)_+ - (d\sigma/d\Omega)_-] / [P^-(d\sigma/d\Omega)_+ + P^+(d\sigma/d\Omega)_-] . \quad (4.13)$$

4.5 Statistical Uncertainty in Differential Cross-Section and Analyzing Power

Writing the differential cross-section from equation (4.8) as

$$(d\sigma/d\Omega) = k\, N , \qquad (4.14)$$

the uncertainty in a measured differential cross-section is given by

$$\delta(d\sigma/d\Omega) = (d\sigma/d\Omega) (N)^{-1/2} , \qquad (4.15)$$

assuming that the uncertainties in the terms contained in k are negligible.

If a number of background counts N_B are subtracted from the total number of counts N_T under the peak of interest in the focal plane spectrum, the differential cross-section given by equation (4.14) becomes

$$(d\sigma/d\Omega) = k (N_T - N_B) \qquad (4.16)$$

and the uncertainty in the differential cross-section is given by

$$\delta(d\sigma/d\Omega) = (d\sigma/d\Omega) (N_T+N_B)^{1/2} / (N_T - N_B) . \qquad (4.17)$$

The uncertainty in $(d\sigma/d\Omega)_o$ is given by

$$\delta((d\sigma/d\Omega)_o)^2 = (\partial (d\sigma/d\Omega)_o /\partial U)^2 (\delta U)^2 + (\partial (d\sigma/d\Omega)_o /\partial D)^2 (\delta D)^2 , \qquad (4.18)$$

where U and D represent the differential cross-sections $(d\sigma/d\Omega)_+$ and $(d\sigma/d\Omega)_-$ respectively. This reduces to

$$\delta((d\sigma/d\Omega)_o) = [(P^- \delta U)^2 + (P^+ \delta D)^2]^{1/2} / [P^+ + P^-] . \qquad (4.19)$$

Similarly, the uncertainty in analyzing power may be written as

$$\delta A = [(P^+ + P^-) / (P^-U + P^+D)^2] [(D\delta U)^2 + (U\delta D)^2]^{1/2} . \qquad (4.20)$$

Equations (4.19) and (4.20) have been derived assuming that there is no uncertainty in the polarization measurements.

4.6 Normalization

A series of calibration runs were performed at each angle to determine the differential cross-section for elastic scattering from ^{48}Ca. The elastic prescaler was reduced and the MRS front end trigger requirement set to (X_o or Y_o) to allow calculation of the overall MRS efficiency. For the remainder of the experiment, data was collected with the MRS front end trigger set to (X_o and Y_o) and the prescaler increased to supress the elastic peak relative to the inelastic peak corresponding to the M1 transition. By calculating the ratio of the inelastic to the elastic differential cross-sections in these runs, the differential cross-section of the M1 transition was normalized to the elastic calibration. The analyzing power is independent of any overall normalization in the measured differential cross-sections.

To check the overall normalization of the data, the differential cross-section for the well-known p-p elastic scattering reaction was measured using a CH_2 target. In addition, measurement of the analyzing power for the p-p elastic scattering reaction provides a useful check for instrumental asymmetries. The accepted values of differential cross-section and analyzing power appropriate to this experiment are listed in appendix (4.2).

4.7 Calibration of Scattering Angle

Data from the CH_2 normalization runs were used to calibrate the angular position of the MRS relative to the beam axis by measuring the energy difference between scattering from protons and carbon nuclei in the CH_2 target. The energy difference is dictated by the reaction kinematics governing the two processes. At forward angles, the energy of a proton scattered in the pp elastic scattering reaction is approximately equal to that of a proton which excites the first excited state of carbon, with $J^{\pi}=2^{+}$ at 4.44 MeV, in the ^{12}C (p,p')$^{12}C^{*}$ reaction. The kinematics of the two reactions at an incident beam energy of 250 MeV, are illustrated in figure (4.5).

An experiment with a CH_2 target in place was performed at the crossing angle. In the replay analysis, the data was divided into small angular bins and the two peaks were

resolved in order to find the Y_o channel which corresponds to the crossing angle. With this knowledge, the angle of any other Y_o channel, or the centre of some Y_o bin, may be calculated directly from the target-FEC geometry.

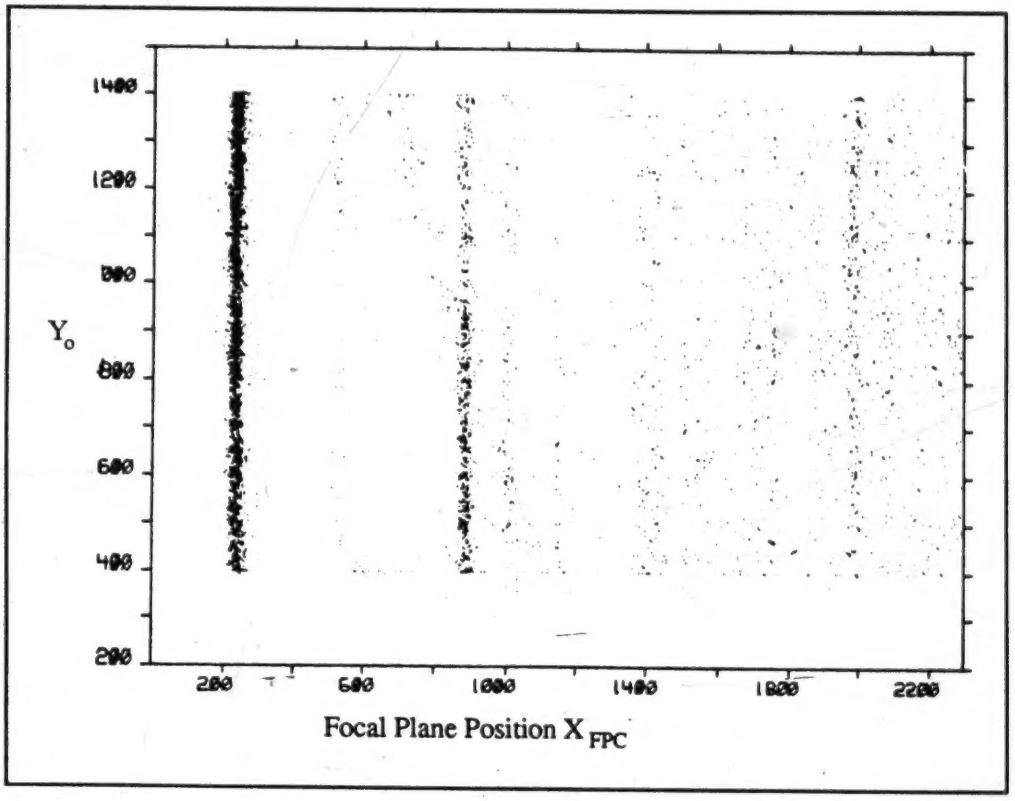

Figure 4.1 Spectrum showing independence of focal plane position on Y_o

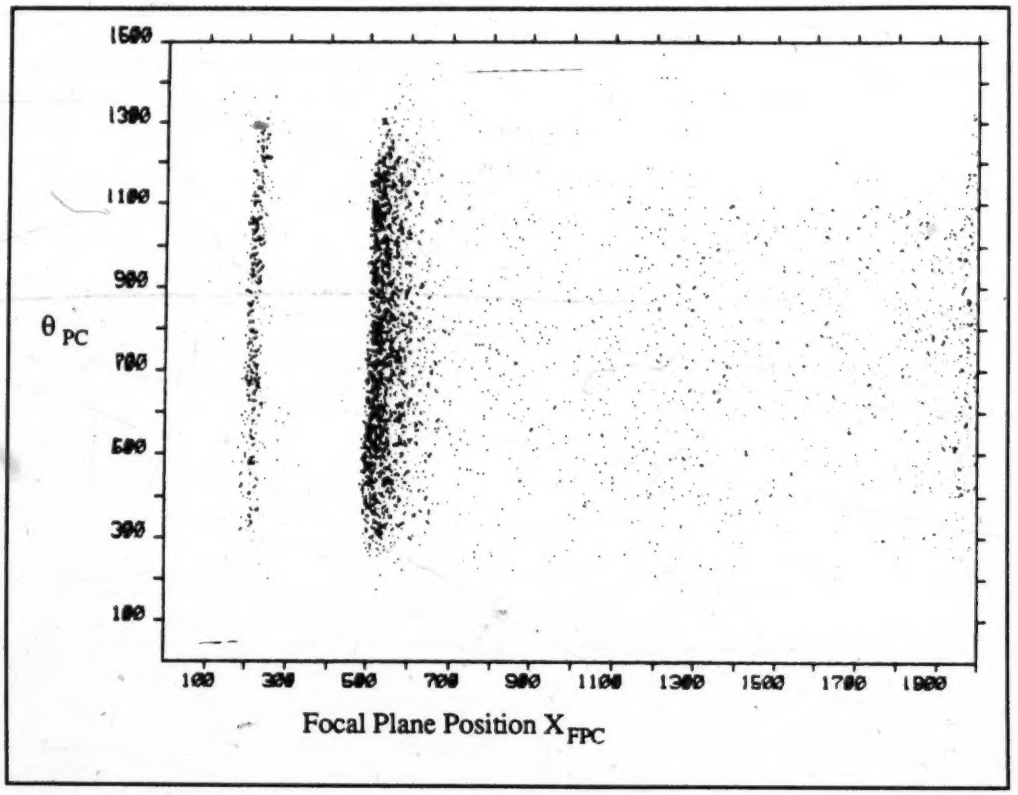

Figure 4.2 Spectrum showing independence of focal plane position on θ_{PC}

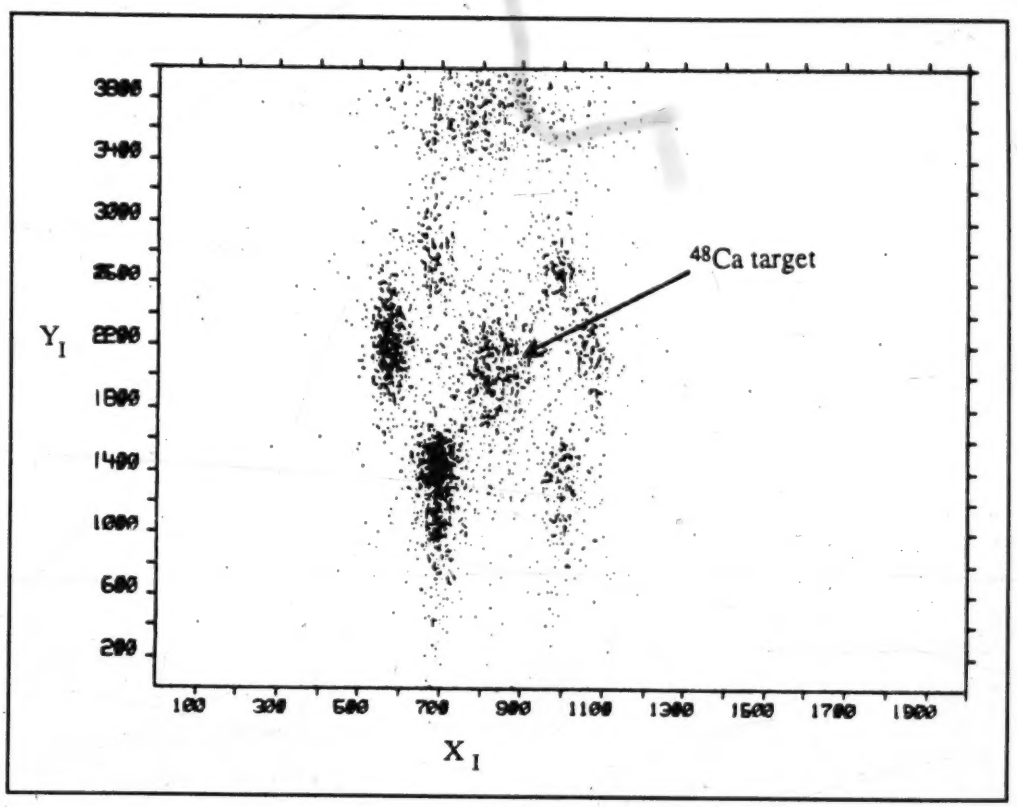

Figure 4.3 Spectrum Y_I vs. X_I showing image of ^{48}Ca target and target frame.

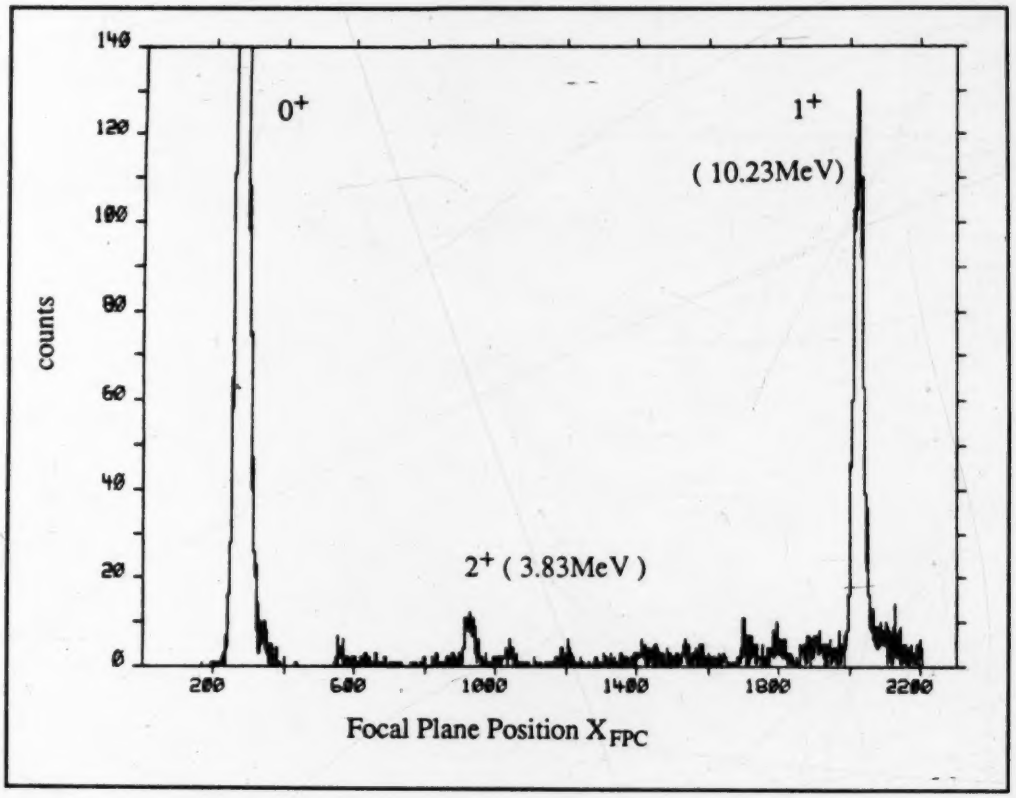

Figure 4.4 Typical Focal Plane Spectrum X_{FPC}

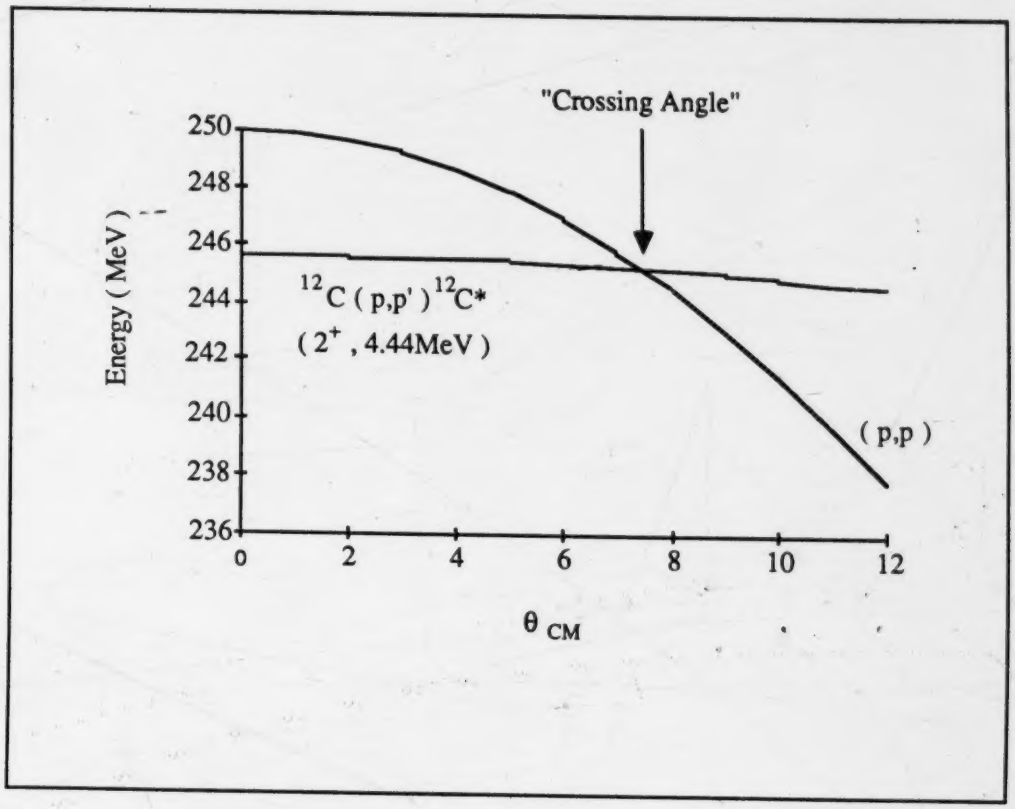

Figure 4.5 Energy of outgoing proton after scattering from CH_2 target at 250 MeV.

5. Results

The ^{48}Ca (p,p')$^{48}Ca^*$ experiment was performed during two separate runs: one in January 1985, at proton beam energies of 319 and 400 MeV, the other in October 1985 at 250 and 500 MeV. The numerical results of the two analyses are listed in appendix (6).

5.1 ^{48}Ca (p,p')$^{48}Ca^*$ at 319 and 400 MeV (January 1985)

Individual focal plane spectra were obtained in the replay analysis for data collected at each energy, scattering angle and MRS trigger requirement, with the beam polarization in the UP, DOWN and OFF spin states. The energy resolution of the spectra was typically 200 keV.

The differential cross-sections and analyzing powers were calculated from the focal plane spectra for the p-p elastic scattering reaction and the ^{48}Ca elastic calibration runs. The differential cross-sections for p-p elastic scattering obtained from the data were not in agreement with the results of the SAID calculations [20] listed in appendix (4.2). Furthermore, the ^{48}Ca elastic calibration data did not agree with the DWBA analysis using the DWBA83 computer code [15] described in chapter (2.3b). The code is typically accurate to within 10% of the differential cross-section for the elastic scattering reaction.

The discrepancy lies in the calculation of the overall MRS efficiency, as outlined in chapter (4.3d). The data taken during this run was plagued with an extreme inefficiency in the Y_0 plane of the FEC. Because of the inefficiency, not all of the scattering events would necessarily trigger the MRS electronics, even with the MRS trigger requirement set to (X_0 or Y_0). Moreover, the efficiency was not uniform over the FEC, so that the efficiency calculated over the entire FEC will not represent the true FEC efficiency for events in the solid angle acceptance of the spectrometer. Unfortunately, no method to determine the MRS efficiency over some particular portion of the FEC could be established.

In order to surmount the difficulty associated with the calculation of the overall MRS efficiency, the CH_2 data was normalized to the accepted p-p elastic cross-section at each energy and angle. The overall MRS efficiencies required to reproduce the accepted p-p elastic cross-sections were 74% at 319 MeV and 68% at 400 MeV, both of which are typically achieved by the MRS.

With the assumption that the MRS efficiency did not change between the CH_2 and the ^{48}Ca elastic scattering runs, the ^{48}Ca elastic calibration cross-sections were normalized, with the CH_2 data, to the accepted p-p elastic scattering values. This is a reasonable assumption since the two runs were carried out sequentially. The differential cross-section and analyzing power for proton elastic scattering on ^{48}Ca at 319 MeV are presented in figures (5.1) and (5.2) respectively. The values obtained compare well with the results of the DWBA analysis, although there are some small discrepancies in the analyzing power results.

The differential cross-section of the M1 transition in ^{48}Ca (p,p')$^{48}Ca^*$ reaction at 319 MeV was normalized to the elastic calibration, as described in chapter (4.6). In figure (5.3), the experimental results are compared to the IPM strength predicted with the DWBA analysis. The IPM strength must be normalized by a factor of N=0.25 to agree with the experimentally observed values. This agrees well with previous experimental data [7, 8] and the normalizations of the IPM strength (N=0.29 and N=0.28 respectively) from the DWIA analyses described therein.

The analyzing power of the M1 transition at 319 MeV is presented in figure (5.4). The error bars include statistical uncertainties only. There is a large discrepancy between the data and the results of the DWBA calculation.

The DWBA curve presented in figure (5.4) is similar in magnitude to the results of the DWIA analyses [7,8] but opposite in sign. Since the calculation of analyzing power for inelastic scattering processes is extremely sensitive to the choice of nuclear wave functions and the method of calculation, large disagreements between various calculations are common [17,14]. It is not surprising, therefore, that large discrepancies between experiment and theory are observed.

Previously, evidence of structure (a large dip) in the angular distribution of analyzing power at 319 MeV was reported [7] at a scattering angle of 5°. The experiment was repeated at 340 MeV [8] but no structure was observed. The results of this experiment might show some evidence of structure at 4°, but this is inconclusive because of the large statistical uncertainties in the experimental data.

The differential cross-section, normalized to the CH_2 data, and analyzing power of the ^{48}Ca elastic scattering reaction at 400 MeV are presented in figures (5.5) and (5.6) respectively. The differential cross-section data is in good agreement with the DWBA analysis. The theoretical and experimental results for the analyzing power are in poor agreement.

The differential cross-section of the M1 transition at 400 MeV, normalized to the

^{48}Ca elastic scattering cross-section, is compared to the prediction of the IPM in figure (5.7). The IPM strength must be normalized by the factor N=0.28 for agreement with the experimental results. The analyzing power of the M1 transition is presented in figure (5.8). The poor agreement between experiment and the DWBA analysis for the analyzing power is expected, given the shortcomings of the analysis described previously.

5.2 ^{48}Ca (p,p')^{48}Ca* at 250 and 500 MeV (October 1985)

The differential cross-sections and analyzing powers calculated for the p-p elastic scattering reaction from this data set were not in agreement with the results of the SAID calculations [20].

On the other hand, the ^{48}Ca elastic scattering calibration data were found to be in good agreement with the results of the DWBA analysis as shown in figures (5.9), (5.10) for 250 MeV and figures (5.13) and (5.14) for 500 MeV, although there is some small disagreement between experiment and theory for the analyzing power at 500 MeV. However, both the differential cross-section and analyzing power at 500 MeV are in excellent agreement with results published previously [18]. The results for the p-p elastic and ^{48}Ca elastic calibrations were both obtained using the same standard MRS efficiency calculations.

Since the disagreement between the p-p elastic scattering data and the SAID calculations was most likely due to uncertainty in the target's composition, the differential cross-section of the M1 transition was normalized to the ^{48}Ca elastic scattering calibration according to chapter (4.6).

In figure (5.11), the differential cross-section for the M1 transition at 500 MeV is compared to the IPM prediction. The IPM strength must be normalized by a factor of N=0.6 to obtain agreement with experiment. At 250 MeV, the IPM strength of the M1 transition was found to require a normalization factor of about N=0.3, as illustrated in figure (5.15). The analysis at 500 MeV was complicated by limited statistics for the M1 peak and the presence of a large amount of background in the focal plane spectra.

The analyzing powers for the M1 transition at 250 and 500 MeV are presented in figures (5.12) and (5.16) respectively. The disagreements between the data and the DWBA analyses are similar to 319 and 400 MeV cases.

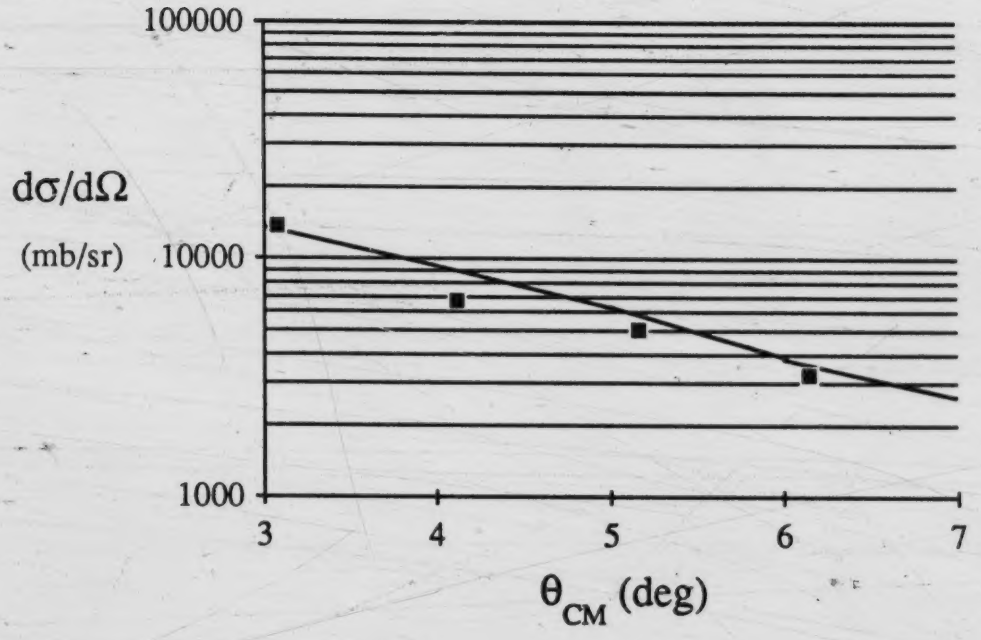

Figure 5.1 Angular distribution of differential cross-section for proton elastic scattering from ^{48}Ca at 319 MeV.

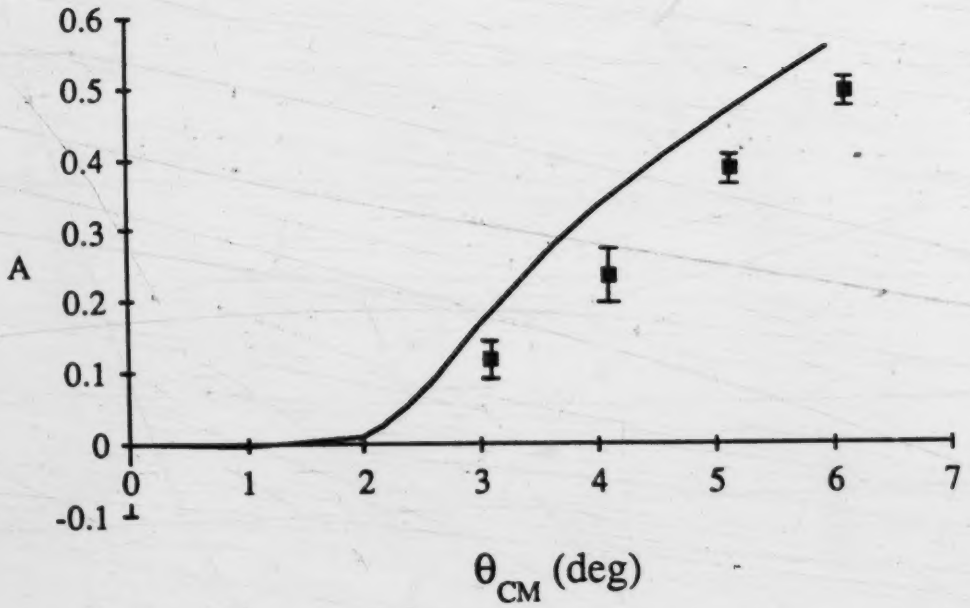

Figure 5.2 Angular distribution of analyzing power for proton elastic scattering from ^{48}Ca at 319 MeV.

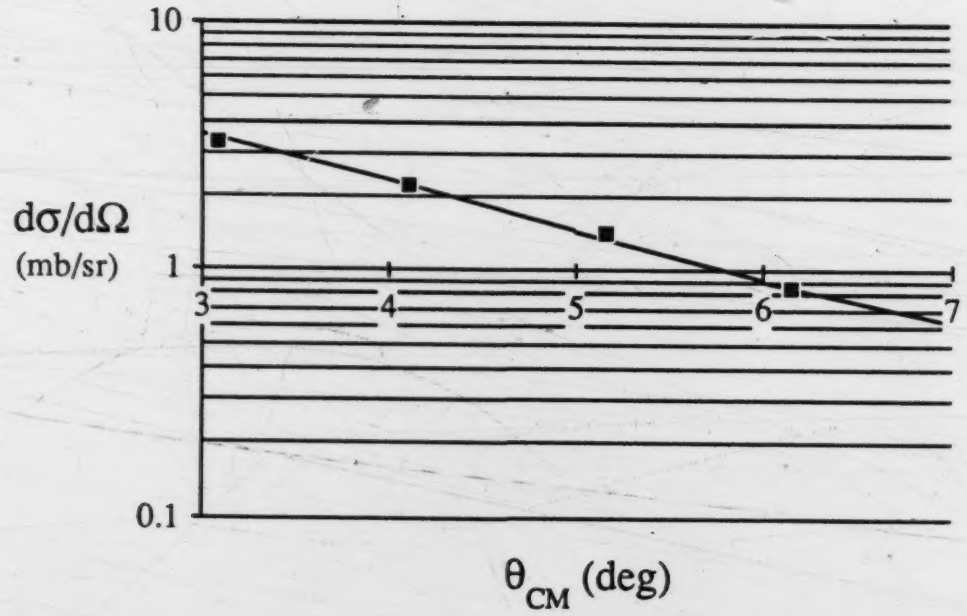

Figure 5.3 Angular distribution of differential cross-section for M1 transition excited in ^{48}Ca (p,p')^{48}Ca* reaction at 319 MeV. The DWBA curve has been normalized by a factor N=0.25 to obtain agreement with experiment.

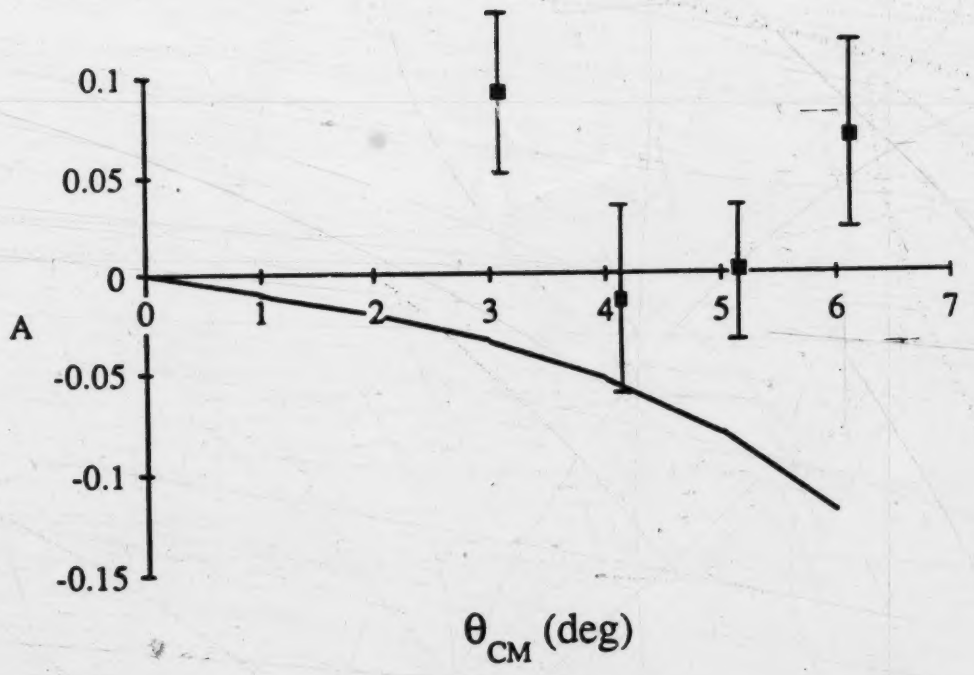

Figure 5.4 Angular distribution of analyzing power of M1 transition excited in the ^{48}Ca (p,p')$^{48}Ca^{*}$ reaction at 319 MeV.

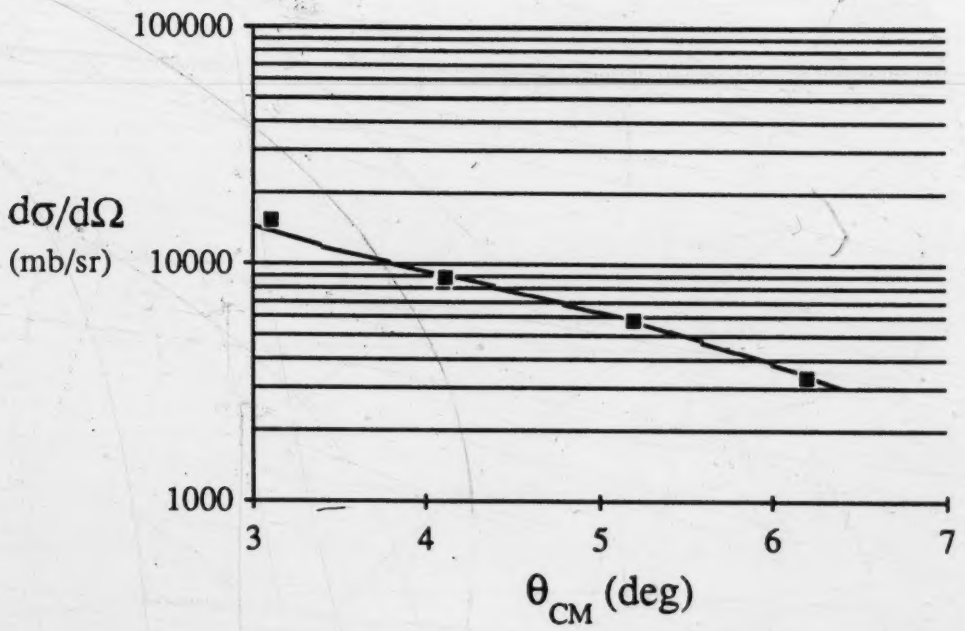

Figure 5.5 Angular distribution of differential cross-section for proton elastic scattering from ^{48}Ca at 400 MeV.

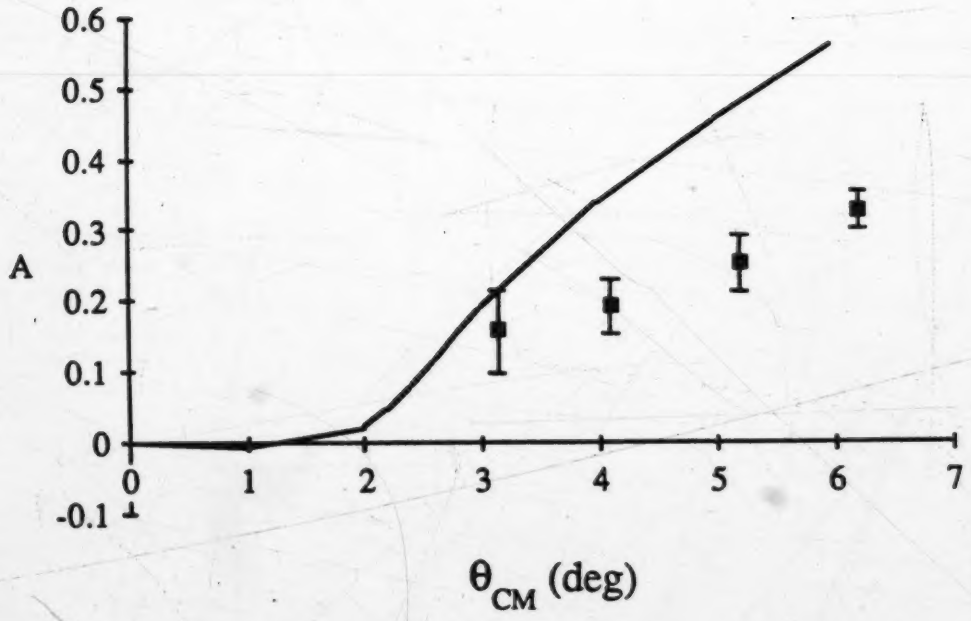

Figure 5.6 Angular distribution of analyzing power for proton elastic scattering from ^{48}Ca at 400 MeV.

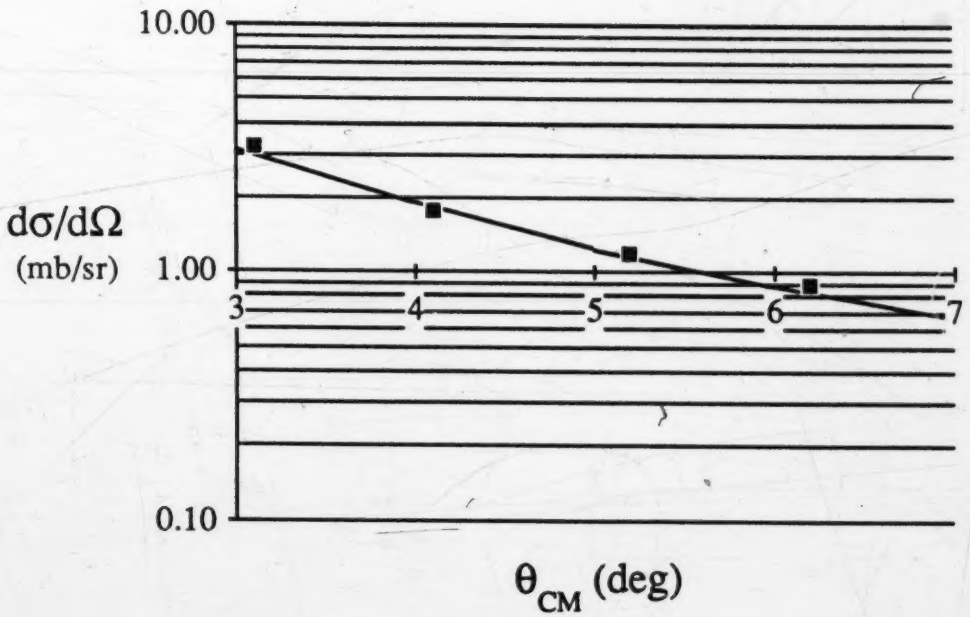

Figure 5.7 Angular distribution of differential cross-section for M1 transition excited in ^{48}Ca (p,p')$^{48}Ca^{*}$ reaction at 400 MeV. The DWBA curve has been normalized by a factor N=0.28 to obtain agreement with experiment.

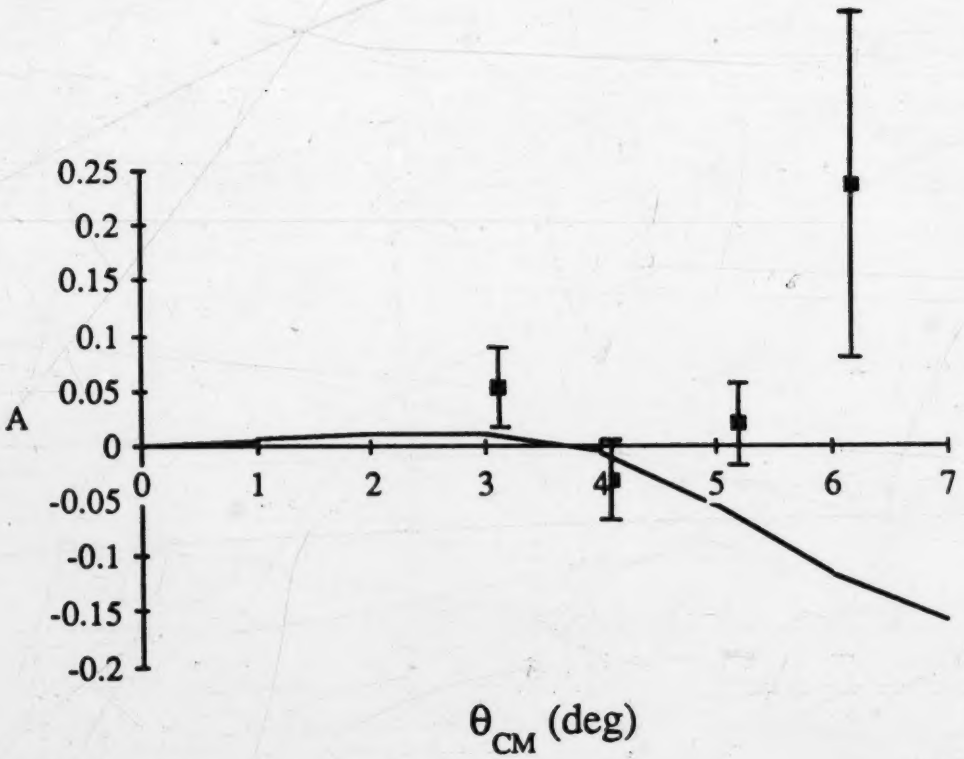

Figure 5.8 Angular distribution of analyzing power of M1 transition excited in ^{48}Ca (p,p')$^{48}Ca^{*}$ reaction at 400 MeV.

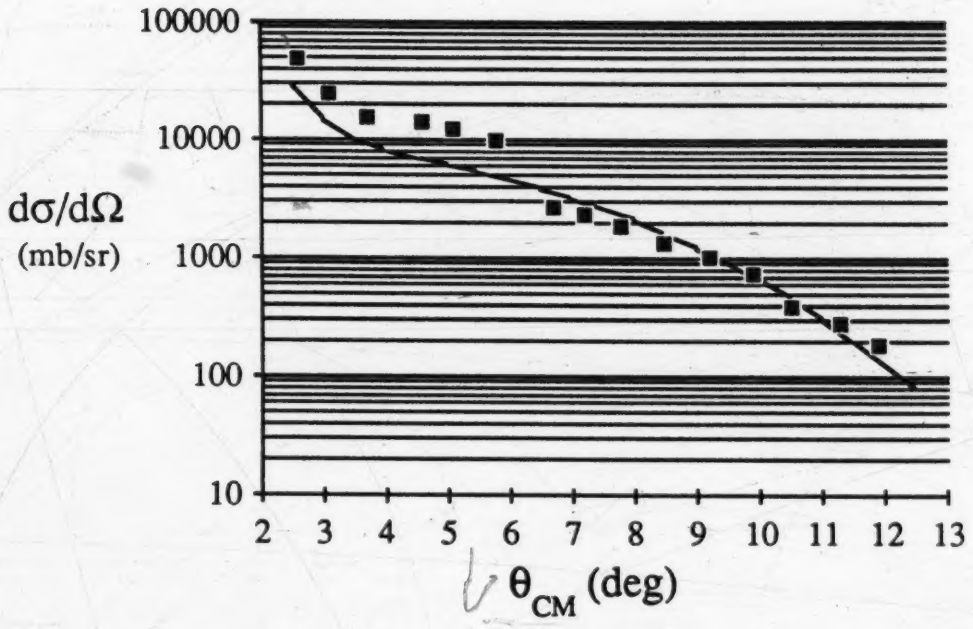

Figure 5.9 Angular distribution of differential cross-section for proton elastic scattering from ^{48}Ca at 250 MeV.

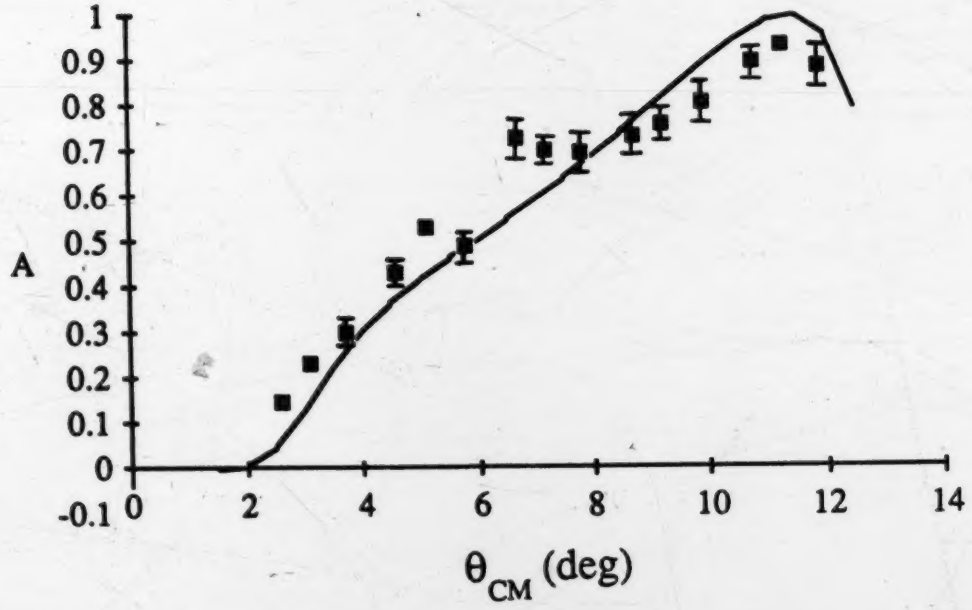

Figure 5.10 Angular distribution of analyzing power for proton elastic scattering from ^{48}Ca at 250 MeV.

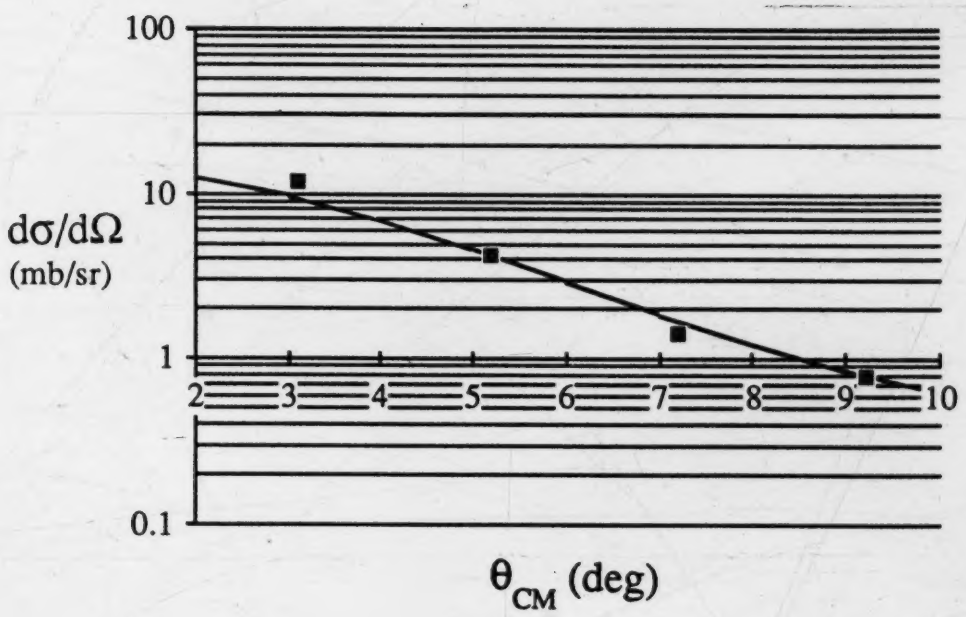

Figure 5.11 Angular distribution of differential cross-section for M1 transition excited in ^{48}Ca (p,p')$^{48}Ca^{*}$ reaction at 250 MeV. The DWBA curve has been normalized by a factor N=0.6 to obtain agreement with experiment.

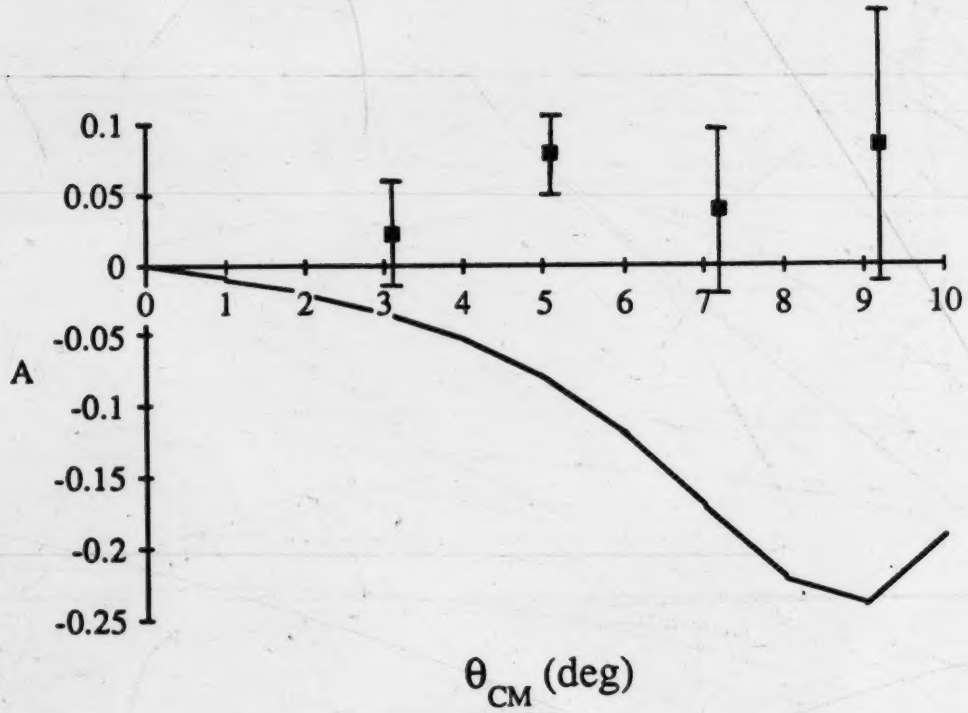

Figure 5.12 Angular distribution of analyzing power of M1 transition excited in the ^{48}Ca (p,p')$^{48}Ca^{*}$ reaction at 250 MeV.

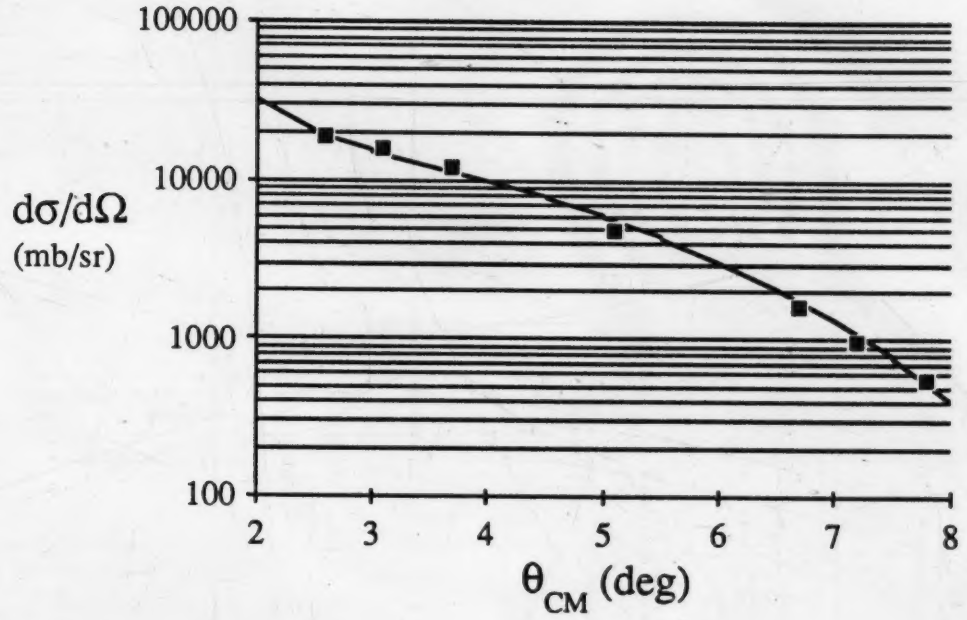

Figure 5.13 Angular distribution of differential cross-section for proton elastic scattering from ^{48}Ca at 500 MeV.

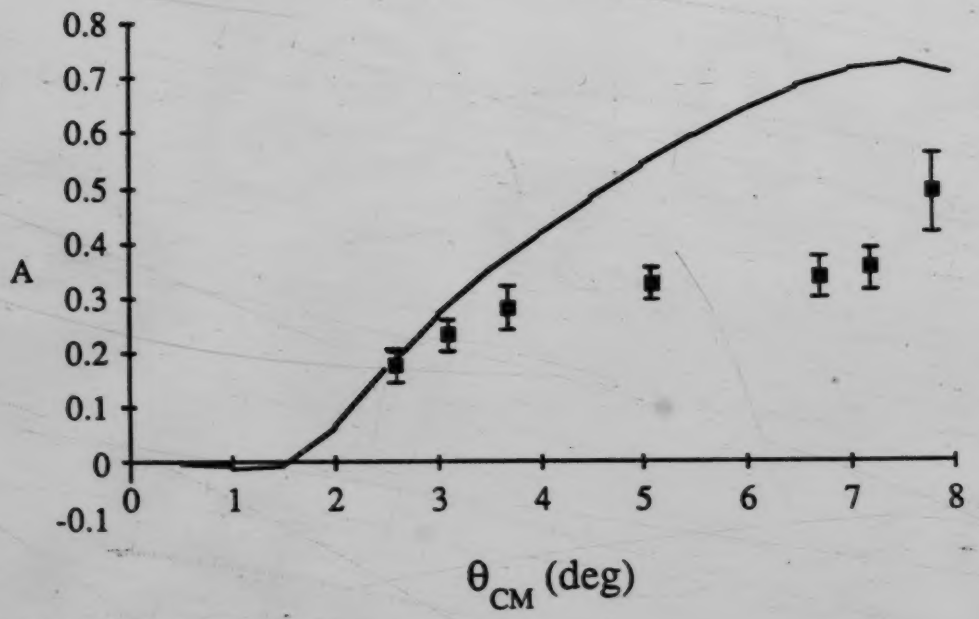

Figure 5.14 Angular distribution of analyzing power for proton elastic scattering from ^{48}Ca at 500 MeV.

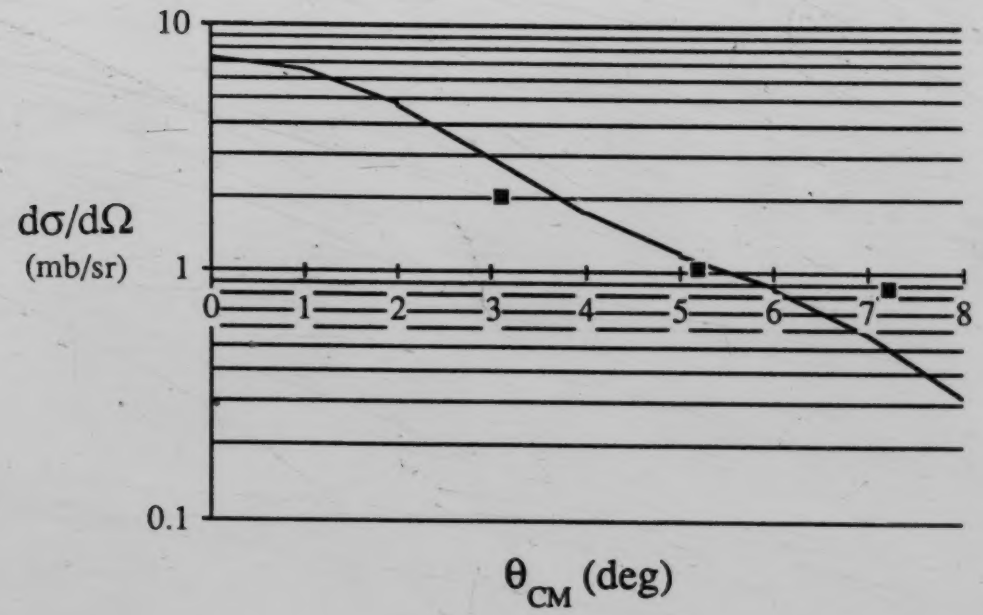

Figure 5.15 Angular distribution of differential cross-section for M1 transition excited in ^{48}Ca (p,p')$^{48}Ca^{*}$ reaction at 500 MeV. The DWBA curve has been normalized by a factor N=0.3 to obtain agreement with experiment.

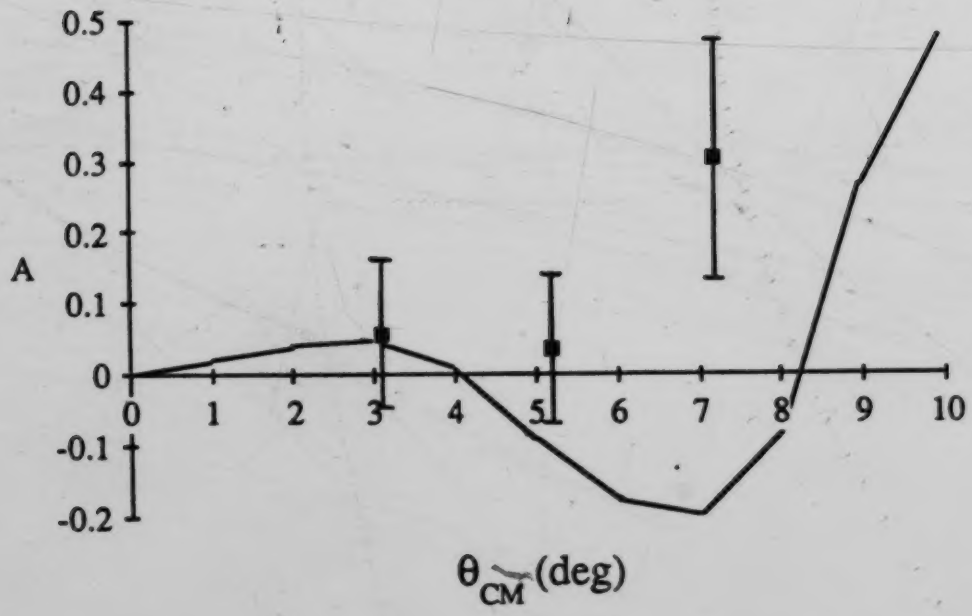

Figure 5.16 Angular distribution of analyzing power of M1 transition excited in ^{48}Ca (p,p')$^{48}Ca^{*}$ reaction at 500 MeV.

6. Discussion

The quenching of M1 transition strength in the ^{48}Ca (p,p')^{48}Ca* reaction has been previously studied over an energy range extending from 44 to 334 MeV [3-8]. In all of the previous work, the estimate of the M1 strength based on the independent particle model (IPM) had to be renormalized by a factor of about N=0.3 to obtain agreement with the experimentally measured differential cross-sections. The results of this work extend the energy range of the investigation up to 500 MeV.

At incident beam energies of 319, 400 and 500 MeV, the measured M1 strength was found to be quenched by the same factor, of about N=0.3, as observed in the previous studies.

At 250 MeV however, the amount of quenching observed was reduced to N=0.6 of the IPM strength. In view of the apparent energy-independence of the quenching indicated by the other data, the amount of quenching at 250 MeV measured in this experiment is anomalously small. To check the validity of the IPM calculations at increasingly lower energies, the microscopic DWBA analysis was carried out for the ^{48}Ca (p,p')^{48}Ca* reaction at 200 MeV. A normalization factor of N=0.3 was required to obtain agreement with previous data [6]. The reliability of the 250 MeV data is thereby called into question. Since this type of anomalous behaviour would prove to be an important result, the M1 transition strength in the ^{48}Ca (p,p')^{48}Ca* reaction at 250 MeV warrants experimental reinvestigation.

The analyzing power of the M1 transition was measured and compared to the IPM. Since the results of the calculations are extremely sensitive to the choice of wave functions representing the initial and final nuclear states, little information may be gained from the study of this spin-observable at the present time. These measurements are important, however, since the extreme sensitivity to the nuclear wave functions will undoubtedly provide an important tool for future theoretical investigations.

The quenching of the M1 transition strength in the ^{48}Ca (p,p')^{48}Ca* reaction is not unique. In a series of studies, the M1 transition strengths in (p,p') reactions at 200 MeV on a variety of nuclei, ranging from ^{28}Si to ^{140}Ce, were quenched by at least 50% from the IPM strength [21-24].

In studies which measure the M1 transition strength excited with (e,e') reactions, the M1 transition strength is typically quenched by more than 50% from the IPM strength [eg. ref. 2]. Since electrons do not interact strongly, (e,e') studies are particularly welcome since there is no possibility that the target nucleus will be distorted

by the incoming electron. Furthermore, since the electromagnetic M1 transition operator for an (e,e') reaction is well known from electromagnetic theory, (e,e') studies provide direct information about the nuclear structure. This may be used in conjunction with the results of (p,p') experiments to obtain information about the $V_{\sigma\tau}$ term in the effective NN interaction.

The Gamow-Teller strength, in (p,n) reactions, which is the analogue of the M1 transition strength, has also been used as a probe of nuclear structure. Like the M1 transition, the Gamow-Teller transition is excited by the $V_{\sigma\tau}$ term in the effective NN interaction. Quenching of the Gamov-Teller strength by more than 50% from the IPM strength is observed in (p,n) reactions [25].

In all of these studies, a large part of the quenching is understood to arise from weaknesses in the IPM itself. The residual interaction, not included in the IPM, causes configuration mixing among both proton and neutron IPM levels. This conventional nuclear structure effect leads to a reduction of the IPM strength. Configuration mixing alone, however, can not account for all of the "missing" M1 transition strength.

It is generally accepted that the remainder of the "missing" M1 strength is exhausted by exciting one of the nucleons into a Δ-nucleon hole state, but the actual contribution from this quenching mechanism remains somewhat controversial.

At this point, it is advisable to mount a theoretical effort to calculate M1 transition strengths, within a single framework, for the large data set now available. With an increased understanding of nuclear structure involved in the reactions, the isovector spin-dependent central part of the nucleon-nucleon interaction $V_{\sigma\tau}$ could be extracted.

References

1. W.G. Love and M.A. Franey, Phys. Rev. **C24**, 1073 (1981).
2. W. Steffan *et al.*, Phys. Lett. **95B**, 23 (1980).
3. Y. Fujita *et al.*, Phys. Rev. **C25**, 678 (1982).
4. G.P.A. Berg *et al.*, Phys. Rev. **C25**, 2100 (1982).
5. K.E. Rehm *et al.*, Phys. Lett. **114B**, 15 (1982).
6. G.M. Crawley *et al.*, Phys. Lett. **127B**, 322 (1983).
7. S.K. Nanda *et al.*, Phys. Rev. **C29**, 660 (1984).
8. D.J. Horen *et al.*, Phys. Rev. **C31**, 2049 (1985).
9. G.F. Bertsch, Nuc. Phys. **A354**, 157c (1981).
10. J.B. McGrory and B.H. Wildenthal, Phys. Lett. **103B**, 173 (1981).
11. W. Knupfer, B.C. Metsch and A. Richter, Phys. Lett. **129B**, 375 (1983).
12. L. Chaves and A. Poves, Phys. Lett. **171B**, 343 (1986).
13. W. Weise, Nuc. Phys. **A396**, 373 (1983).
14. L. Rikus, K. Nakano and H.V. Von Geramb, Nuc. Phys. **A414**, 413 (1984).
15. from program DWBA70, R. Schaeffer and J. Raynal (unpublished).
16. D. Frekers, TRIUMF (unpublished).
17. R. Dymarz, University of Alberta, private communication ;
    see for example J.R. Comfort *et al.*, Phys. Rev. **C26**, 1800 (1982) to compare DWIA calculations to DWBA calculations of ref. [14] for ^{12}C (p,p')$^{12}C^*$.
18. K.K. Seth *et al.*, Phys. Lett. **158B**, 23 (1985).
19. G. Greeniaus, University of Alberta (unpublished).
20. R.A. Arndt, Interactive Dial-in program *SAID* (unpublished).
21. N. Anantaraman *et al.*, Phys. Rev. Lett. **52**, 1409 (1984).
22. C. Djalali *et al.*, Nuc. Phys. **A388**, 1 (1982).
23. G.M. Crawley *et al.*, Phys. Rev. **C26**, 87 (1982).
24. C. Djalali *et al.*, Phys. Rev. **C31**, 758 (1985).
25. B.D. Anderson *et al.*, Phys. Rev. Lett. **45**, 699 (1980).

Bibliography

Brussaard P.J. and Glaudemans P.W.M., **Shell - Model applications in nuclear spectroscopy**, North-Holland (1977).

Jackson D.F., **Nuclear Reactions**, Methuen (1970).

Appendix 1

Formal Scattering Theory

To solve the problem of potential scattering of a projectile from a target, the time-independent Schrödinger equation

$$H|\Psi> = E|\Psi> \qquad (A1.1)$$

must be solved subject to the condition that the asymptotic solutions behave like an incoming plane wave and an outgoing spherical wave. If the total Hamiltonian H is written as the sum of the kinetic energy operator H_o and the projectile-target interaction V, the Schrödinger equation may be expressed as

$$(E - H_o)|\Psi> = V|\Psi> . \qquad (A1.2)$$

In the absence of a potential, the problem becomes

$$(E - H_o)|\phi> = 0 , \qquad (A1.3)$$

where the $|\phi>$ states represent plane waves. The general solution of equation (A1.2) is obtained by applying an operator defined by

$$G_o^{\pm} \equiv (E - H_o \pm i\varepsilon)^{-1} \qquad (A1.4)$$

and adding any solution of (A1.3) to obtain the Lipmann-Schwinger equation,

$$|\Psi^{\pm}> = |\phi> + G_o^{\pm} V |\Psi^{\pm}>. \qquad (A1.5)$$

The scattering state $|\Psi^{+}>$ represents an outgoing spherical wave, while $|\Psi^{-}>$ represents the time reversed incoming spherical wave.

In analogy with the operator $G_o^{\pm}$ defined by relation (A1.4), an operator $G^{\pm}$ corresponding to the total Hamiltonian H can be defined as

$$G^{\pm} \equiv (E - H \pm i\varepsilon)^{-1} . \qquad (A1.6)$$

Using the operator identity

$$(A)^{-1} - (B)^{-1} = (B)^{-1}(B - A)(A)^{-1}, \qquad (A1.7)$$

it is possible to express $G_o^{\pm}$ in terms of $G^{\pm}$ as

$$G_o^{\pm} = G^{\pm}(1 - V G_o^{\pm}) . \qquad (A1.8)$$

By substituting equation (A1.8) into (A1.5) the formal solution of the Lipmann-Schwinger equation is obtained

$$|\Psi^{\pm}> = (1 + G^{\pm} V)|\phi> . \qquad (A1.9)$$

The transition operator appearing in equation (1.1) is defined formally by

$$T^{\pm} \equiv V(1 + G^{\pm} V) \qquad (A1.10)$$

which may be written alternately as

$$T^{\pm} \equiv V + V G_o^{\pm} T^{\pm} . \qquad (A1.11)$$

The transition matrix element for a scattering process is defined as

$$T_{fi} \equiv <\phi_f | T^{+} | \phi_i> \qquad (A1.12)$$

which becomes

$$T_{fi} = <\phi_f | V | \Psi_i^{+}>, \qquad (A1.13)$$

by substituting for T from equation (A1.10) and using the Lipmann-Schwinger equation (A1.9). From equation (A1.13), it is possible to construct the transition matrix element for a scattering reaction which proceeds through a potential V.

Now consider the case where the potential V can be separated into two terms V=U+W such that the scattering problem with the potential U has a known solution $|\chi^{\pm}>$ which obeys

$$(E - H_o - U)\,|\,\chi^{\pm}\rangle = 0\,. \qquad (A1.14)$$

Using the formal solution of the Lipmann-Schwinger equation (A1.9), it is possible to write

$$|\,\chi^{\pm}\rangle = (1 + G_U^{\pm} U)\,|\,\phi\rangle\,, \qquad (A1.15)$$

where $G_U^{\pm}$ is defined by

$$G_U^{\pm} \equiv (E - H_o - U \pm i\varepsilon)^{-1}\,. \qquad (A1.16)$$

Similarly, the complete scattering problem with the potential V = U+W

$$(E - H_o - U - W)\,|\,\Psi^{\pm}\rangle = 0\,, \qquad (A1.17)$$

may be solved by

$$|\,\Psi^{\pm}\rangle = |\,\phi\rangle + G^{\pm}(U+W)\,|\,\phi\rangle\,. \qquad (A1.18)$$

Using the identity (A1.7), it is possible to express the operator $G^{\pm}$ in terms of $G_U^{\pm}$ as

$$G^{\pm} = G_U^{\pm} + G_U^{\pm} W G^{\pm} \qquad (A1.19)$$

and substitute this into equation (A1.18) to obtain the result

$$|\,\Psi^{\pm}\rangle = |\,\phi\rangle + (G_U^{\pm} + G_U^{\pm} W G^{\pm})\,(U+W)\,|\,\phi\rangle\,, \qquad (A1.20)$$

which, with equation (A1.15), ultimately reduces to

$$|\,\Psi^{\pm}\rangle = |\,\chi^{\pm}\rangle + G_U^{\pm} W\,|\,\Psi^{\pm}\rangle\,. \qquad (A1.21)$$

The transition matrix element for this scattering problem may be written in accordance with equation (A1.13) as

$$T_{fi} = \langle \phi_f\,|\,U + W\,|\,\Psi_i^{+}\rangle\,, \qquad (A1.22)$$

which becomes

$$T_{fi} = \langle \phi_f | U | \chi_i^+ \rangle + \langle \phi_f | W | \chi_i^+ \rangle + \langle \phi_f | UG_U^+ W | \Psi_i^+ \rangle$$

$$+ \langle \phi_f | WG_U^+ W | \Psi_i^+ \rangle , \qquad (A1.23)$$

by substituting for $| \Psi_i^+ \rangle$ from equation (A1.21). Using $G^- = (G^+)^\dagger$ and equation (A1.15) it is possible to write

$$\langle \phi | UG_U^+ = \langle \chi^- | - \langle \phi | . \qquad (A1.24)$$

With this relation, the third term in equation (A1.23) reduces to

$$\langle \phi_f | U G_U^+ W | \Psi_i^+ \rangle = \langle \chi_f^- | W | \Psi_i^+ \rangle - \langle \phi_f | W | \Psi_i^+ \rangle \qquad (A1.25)$$

and similarly the fourth term becomes

$$\langle \phi_f | WG_U^+ W | \Psi_i^+ \rangle = \langle \phi_f | W | \Psi_i^+ \rangle - \langle \phi_f | W | \chi_i^+ \rangle . \qquad (A1.26)$$

The transition matrix element (A1.13) for a separable potential V=U+W may be written as

$$T_{fi} = \langle \phi_f | U | \chi_i^+ \rangle + \langle \chi_f^- | W | \Psi_i^+ \rangle , \qquad (A1.27)$$

which forms the basis for a variety of approximation methods used in scattering problems.

Appendix 2

Approximate methods for inelastic scattering

1. Distorted Wave Born Approximation (DWBA)

Consider a general scattering reaction of the form a + A → b + B , which proceeds through a separable interaction V=U+W . The potential U is taken to be the elastic scattering potential and its solutions $|\chi^{\pm}>$ correspond to plane waves distorted by the potential U. The transition matrix element for such a process may be written in accordance with equation (A1.27) as

$$T_{fi} = <\phi_f\ \xi_f | U | \chi_i^+ \xi_i> + <\chi_f^-\ \xi_f | W | \Psi_i^+\ \xi_i> , \qquad (A2.1)$$

where the labels i and f refer to the initial (a+A) and final (b+B) channels respectively, and ξ denotes the internal coordinates of the particles in a given channel. Since U is taken to be the elastic scattering potential, it connects only identical states and the matrix element for an inelastic process reduces to

$$T_{fi} = <\chi_f^-\ \xi_f | W | \Psi_i^+\ \xi_i> \qquad \text{for } i \neq f. \qquad (A2.2)$$

By iterating equation (A1.21), it is possible to obtain a series expansion for $|\Psi_i^+\ \xi_i>$ which may be written as

$$|\Psi_i^+\ \xi_i> = \sum_n (G_U^+ W)^n |\chi_i^+\ \xi_i> , \qquad (A2.3)$$

and substituted into equation (A2.2) to obtain the Born series expansion of the transition matrix element for an inelastic reaction

$$T_{fi} = <\chi_f^-\ \xi_f | W | \chi_i^+ \xi_i> + <\chi_f^-\ \xi_f | W\, G_U^+ W | \chi_i^+ \xi_i> + \ldots \qquad (A2.4)$$

The Distorted Wave Born Approximation (DWBA) is made by neglecting all but the first term in the series to yield

$$T_{fi} = <\chi_f^-\ \xi_f | W | \chi_i^+ \xi_i> , \qquad (A2.5)$$

for an inelastic reaction.

2. Distorted Wave Impulse Approximation. (DWIA)

Instead of solving iteratively for the state $|\Psi_i^+ \xi_i>$ which appears in equation (A2.2) as in the DWBA case, $|\Psi_i^+ \xi_i>$ may be written as

$$|\Psi_i^+ \xi_i> = (1 + G^+ W) |\chi_i^+ \xi_i> , \qquad (A2.6)$$

so that the transition matrix element for an inelastic collision (A2.2) becomes

$$T_{fi} = <\chi_f^- \xi_f | W (1+ G^+ W) | \chi_i^+ \xi_i > . \qquad (A2.7)$$

By defining a transition operator t to describe the scattering of the projectile by the potential U as

$$t \equiv W + W G^+ W , \qquad (A2.8)$$

equation (A2.7) may be written as

$$T_{fi} = <\chi_f^- \xi_f | t | \chi_i^+ \xi_i > . \qquad (A2.9)$$

It is also possible to define a similar transition operator

$$t_j \equiv w_j + w_j G^+ w_j \qquad (A2.10)$$

which describes the scattering of the projectile by the jth nucleon in the target nucleus. Assuming that no multiple scattering processes take place, the transition operator t may be taken to be

$$t = \Sigma_j t_j , \qquad (A2.11)$$

so that the matrix element (A2.2) may be written as

$$T_{fi} = < \chi_f^- \ \xi_f | \sum_j t_j | \chi_i^+ \ \xi_i > \ . \qquad (A2.12)$$

In analogy with equation (A2.10), it is possible to define a transition operator for the scattering of free particles

$$t_j^o \equiv W + W \, G_o^+ W \qquad (A2.13)$$

where G_o^+ is defined by equation (A1.4). The impulse approximation is made by replacing the transition operator in equation (A2.12) with the free transition operator (A2.13) to obtain the Distorted Wave Impulse Approximation (DWIA) expressed as

$$T_{fi} = < \chi_f^- \ \xi_f | \sum_j t_j^o | \chi_i^+ \ \xi_i > . \qquad (A2.14)$$

Appendix 3

In-Beam-Polarimeter properties

1. Beam Polarization

The polarization of the beam, normal to the scattering plane, is determined from the counting asymmetry in the IBP using

$$P = (1 / A) [L - R] / [L + R] . \qquad (A3.1)$$

L and R denote the number of counts in the left and right detectors of the polarimeter respectively and A is the effective analyzing power of the CH_2 polarimeter target.

Energy (MeV)	A (CH_2)
250	0.344
319	0.400
400	0.434
500	0.466

2. Beam Flux

The beam flux I is determined from the total number of counts in the left and right polarimeter detectors

$$I = (L + R) (\#\ \text{protons / count}) , \qquad (A3.2)$$

where

$$(\#\ \text{protons / count}) = [(\text{Rate})(\text{target thickness}) (10^{9}) (1.6 \times 10^{-19})]^{-1} , \qquad (A3.3)$$

for the rate given in units of (counts / sec / nA / mg / cm^2) and target thickness in (mg/cm^2).

Energy (MeV)	Rate	thickness	# protons / count
250	49.053	1.43	8.899×10^7
		28.43	4.476×10^6
319	53.155	2.616	4.489×10^7
400	59.488	2.616	4.011×10^7
500	69.571	1.43	6.274×10^7
		28.43	3.156×10^6

Appendix 4

Reaction Kinematics

1. ^{48}Ca (p,p') $^{48}Ca^*$

The kinematics for the ^{48}Ca (p,p') $^{48}Ca^*$ reaction were calculated using the program KIN2BODY [19]. The quantity η is used to convert the solid angle between the lab and centre of mass frames of reference

$$(d\sigma/d\Omega)_{LAB} = \eta (d\sigma/d\Omega)_{CM} , \qquad (A4.1)$$

at a given scattering angle θ. The ^{48}Ca mass was taken to be 44667 MeV.

Lab Energy (MeV)	θ_{Lab}	θ_{CM}	η
250	3.0	3.1	0.9492
	5.0	5.1	0.9493
	7.0	7.2	0.9495
	9.0	9.2	0.9497
	11.0	11.3	0.9500
319	3.0	3.1	0.9464
	4.0	4.1	0.9464
	5.0	5.1	0.9465
	6.0	6.2	0.9466
400	3.0	3.1	0.9432
	4.0	4.1	0.9432
	5.1	5.2	0.9433
	6.0	6.2	0.9434
500	3.0	3.1	0.9392
	5.0	5.2	0.9393
	7.0	7.2	0.9396

2. CH_2 Normalization

The reaction kinematics for the p-p elastic scattering reaction in the CH_2 normalization runs were calculated using the program KIN2BODY [19]. The differential cross-sections and analyzing powers for p-p elastic scattering were obtained from the interactive dial-in program SAID [20].

Lab Energy	θ_{LAB}	θ_{CM}	η	$d\sigma/d\Omega$(mb/sr)	A
250	4.98	10.60	0.2219	3.702	0.184
	7.48	15.91	0.2235	3.608	0.253
	11.48	24.40	0.2275	3.690	0.324
319	7.60	16.42	0.2169	3.829	0.301
400	6.73	14.81	0.2087	4.214	0.306
500	4.89	11.00	0.1989	5.528	0.245
	7.49	16.83	0.2009	5.224	0.350

Appendix 5

Effect of Kinematic Shift on MRS resolution.

To investigate the effect of kinematic shift on the MRS resolution, the energies E of protons scattered elastically through an angle θ at the target in the ^{48}Ca (p,p)^{48}Ca reaction and accepted by the MRS ($\theta \pm \Delta\theta$) were calculated using the kinematics program KIN2BODY [19].

Calculation of the angular acceptance of the MRS was based on the full FEC acceptance and a target-FEC separation of 130 cm. This results in an angular acceptance of $\Delta\theta = 1.8^{\circ}$. The energy spread of elastically scattered protons on the MRS focal plane is given by

$$\text{Width} = E(\theta - \Delta\theta) - E(\theta + \Delta\theta). \qquad (A5.1)$$

^{48}Ca (p,p)^{48}Ca, E_p = 250 MeV

θ_{LAB}	E ($\theta - \Delta\theta$)	E ($\theta + \Delta\theta$)	Width
3.0	250.00 MeV	249.96 MeV	40 keV
4.0	249.99	249.94	50
5.0	249.98	249.92	60
6.0	249.97	249.89	80
7.0	249.95	249.86	90
8.0	249.93	249.83	100

^{48}Ca (p,p)^{48}Ca, E_p = 500 MeV

θ_{LAB}	E ($\theta - \Delta\theta$)	E ($\theta + \Delta\theta$)	Width
3.0	499.99 MeV	499.91 MeV	80 keV
4.0	499.98	499.86	120
5.0	499.96	499.81	150
6.0	499.93	499.75	180
7.0	499.89	499.69	200
8.0	499.84	499.61	230

Appendix 6

^{48}Ca (p,p')$^{48}Ca^*$ Experimental Data

E_p = 250 MeV

	Elastic Calibration		M1 transition	
θ_{CM}	dσ/dΩ (mb/sr)	A	dσ/dΩ (mb/sr)	A
2.6	21723±669	0.144±0.019		
3.1	10722±248	0.227±0.019	11.79±0.33	0.022±0.037
3.7	6767±505	0.296±0.033		
4.6	3418±25	0.429±0.026		
5.1	3026±286	0.527±0.019	4.29±0.10	0.097±0.030
5.8	2416±74	0.489±0.030		
6.7	1175±142	0.724±0.038		
7.2	1015±119	0.700±0.029	1.42±0.06	0.039±0.057
7.8	820±101	0.695±0.040		
8.7	709±25	0.730±0.038		
9.2	535±20	0.758±0.024	0.79±0.06	0.085±0.094
9.9	387±11	0.803±0.038		
10.8	214±2	0.893±0.025		
11.3	151±2	0.931±0.020		
11.9	99±7	0.882±0.037		

E_p = 319 MeV

	Elastic Calibration		M1 transition	
θ_{CM}	dσ/dΩ (mb/sr)	A	dσ/dΩ (mb/sr)	A
3.1	13560±457	0.120±0.020	3.340±0.159	0.076±0.046

4.1	6691±457	0.235±0.037	2.191±0.090	0.012±0.051
5.2	5066±156	0.389±0.020	1.474±0.063	0.030±0.042
6.1	3287±25	0.494±0.020	0.924±0.038	0.126±0.053

E_p = 400 MeV

	Elastic Calibration		M1 transition	
θ_{CM}	dσ/dΩ (mb/sr)	A	dσ/dΩ (mb/sr)	A
3.2	7164±237	0.158±0.055	3.229±0.164	0.053±0.035
4.1	4933±153	0.226±0.039	1.767±0.074	-0.032±0.038
5.2	2808±37	0.246±0.041	1.196±0.044	0.020±0.042
6.2	1774±32	0.367±0.033	0.898±0.099	0.236±0.160

E_p = 500 MeV

	Elastic Calibration		M1 transition	
θ_{CM}	dσ/dΩ (mb/sr)	A	dσ/dΩ (mb/sr)	A
2.6	19142±311	0.178±0.022		
3.1	15638±2804	0.233±0.018	2.02±0.16	0.055±0.115
3.7	12170±507	0.282±0.028		
5.2	4910±88	0.325±0.024	1.04±0.08	0.035±0.109
6.7	1599±6	0.338±0.043		
7.2	958±50	0.353±0.040	0.87±0.11	0.304±0.180
7.8	554±10	0.491±0.072		